
Since January 2020 Elsevier has created a COVID-19 resource centre with free information in English and Mandarin on the novel coronavirus COVID-19. The COVID-19 resource centre is hosted on Elsevier Connect, the company's public news and information website.

Cell Reports

Article

# SARS-CoV-2 Nsp13 encodes for an HLA-E-stabilizing peptide that abrogates inhibition of NKG2A-expressing NK cells

## Graphical abstract

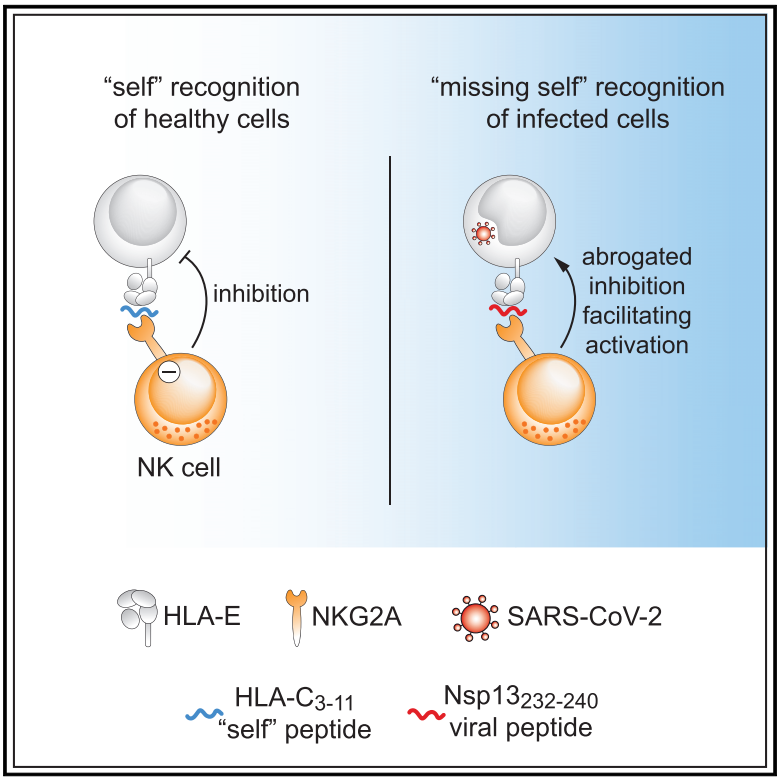


## Highlights

- SARS-CoV-2 Non-structural protein 13 encodes for an HLA-E-restricted peptide
- HLA-E/Nsp13$_{232–240}$ complexes do not bind to the inhibitory receptor NKG2A
- Nsp13$_{232–240}$ allows for NKG2A$^{+}$ NK cell activation by missing self-recognition
- NKG2A$^{+}$ NK cells proficiently restrict SARS-CoV-2 replication *in vitro*

## Authors

Quirin Hammer, Josefine Dunst, Wanda Christ, ..., Jonas Klingström, Hans-Gustaf Ljunggren, Karl-Johan Malmberg

## Correspondence

quirin.hammer@ki.se

## In brief

Natural killer (NK) cells eliminate virus-infected cells. Hammer et al. show that SARS-CoV-2 encodes for a peptide that does not bind to an inhibitory receptor of NK cells, thereby facilitating NK cell activation. This missing self-recognition could enable NK cells to detect and kill SARS-CoV-2-infected cells.

Hammer et al., 2022, Cell Reports *38*, 110503
March 8, 2022 
https://doi.org/10.1016/j.celrep.2022.110503

CellPress

Cell Reports

CellPress
OPEN ACCESS

Article

# SARS-CoV-2 Nsp13 encodes for an HLA-E-stabilizing peptide that abrogates inhibition of NKG2A-expressing NK cells

Quirin Hammer,[1,12,*] Josefine Dunst,[2,3] Wanda Christ,[1] Francesca Picarazzi,[4] Mareike Wendorff,[5] Pouria Momayyezi,[1] Oisín Huhn,[1] Herman K. Netskar,[6,7] Kimia T. Maleki,[1] Marina García,[1] Takuya Sekine,[1] Ebba Sohlberg,[1] Valerio Azzimato,[1] Myriam Aouadi,[1] Karolinska COVID-19 Study Group, Severe COVID-19 GWAS Group, Frauke Degenhardt,[5] Andre Franke,[5] Francesco Spallotta,[8] Mattia Mori,[4] Jakob Michaëlsson,[1] Niklas K. Björkström,[1] Timo Rückert,[9] Chiara Romagnani,[9,10] Amir Horowitz,[11] Jonas Klingström,[1] Hans-Gustaf Ljunggren,[1] and Karl-Johan Malmberg[1,6,7]

[1]Center for Infectious Medicine, Department of Medicine Huddinge, Karolinska Institute, Karolinska University Hospital, Stockholm, Sweden
[2]Division of Immunology and Allergy, Department of Medicine Solna, Karolinska Institute, Karolinska University Hospital, Stockholm, Sweden
[3]Center for Molecular Medicine, Karolinska Institute, Stockholm, Sweden
[4]Department of Biotechnology, Chemistry and Pharmacy, University of Siena, Siena, Italy
[5]Institute of Clinical Molecular Biology, Christian-Albrechts-University of Kiel, Kiel, Germany
[6]Institute of Clinical Medicine, University of Oslo, Oslo, Norway
[7]Department of Cancer Immunology, Institute for Cancer Research, Oslo University Hospital, Oslo, Norway
[8]Institute for Systems Analysis and Computer Science "A. Ruberti," National Research Council (IASI–CNR), Rome, Italy
[9]Innate Immunity, Deutsches Rheuma-Forschungszentrum (DRFZ), Institute of the Leibniz Association, Berlin, Germany
[10]Division of Gastroenterology, Infectiology and Rheumatology, Medical Department I, Charité–Universitätsmedizin Berlin, Berlin, Germany
[11]Department of Oncological Sciences, Precision Immunology Institute, Tisch Cancer Institute, Icahn School of Medicine at Mount Sinai, New York, NY, USA
[12]Lead contact
*Correspondence: quirin.hammer@ki.se
https://doi.org/10.1016/j.celrep.2022.110503

## SUMMARY

Natural killer (NK) cells are innate immune cells that contribute to host defense against virus infections. NK cells respond to severe acute respiratory syndrome coronavirus 2 (SARS-CoV-2) *in vitro* and are activated in patients with acute coronavirus disease 2019 (COVID-19). However, by which mechanisms NK cells detect SARS-CoV-2-infected cells remains largely unknown. Here, we show that the Non-structural protein 13 of SARS-CoV-2 encodes for a peptide that is presented by human leukocyte antigen E (HLA-E). In contrast with self-peptides, the viral peptide prevents binding of HLA-E to the inhibitory receptor NKG2A, thereby rendering target cells susceptible to NK cell attack. In line with these observations, NKG2A-expressing NK cells are particularly activated in patients with COVID-19 and proficiently limit SARS-CoV-2 replication in infected lung epithelial cells *in vitro*. Thus, these data suggest that a viral peptide presented by HLA-E abrogates inhibition of NKG2A$^+$ NK cells, resulting in missing self-recognition.

## INTRODUCTION

Severe acute respiratory syndrome coronavirus 2 (SARS-CoV-2) is a beta-coronavirus that causes coronavirus disease 2019 (COVID-19). In most cases, SARS-CoV-2 infection manifests with mild symptoms, but in some patients the infection develops into severe disease, which can lead to acute respiratory distress syndrome, dysregulated coagulation with thrombosis, multi-organ failure, and death (Guan et al., 2020). The adaptive immune system is central in maintaining long-term protection following infection or vaccination (Sette and Crotty, 2021), and heterogeneous responses of the innate immune system correlate with variable disease outcomes, implying that innate immune cells participate in restraining SARS-CoV-2 replication and thereby potentially shape COVID-19 trajectories (Schultze and Aschenbrenner, 2021).

As part of the innate immune system, natural killer (NK) cells contribute to the control of numerous virus infections (Bjorkstrom et al., 2021). Evidence for this anti-viral activity is presented by patients with genetic deficiencies in NK cell development or NK cell functions, who are more susceptible to certain virus infections (Orange, 2013). In contrast with adaptive lymphocytes, NK cells do not use rearranged antigen receptors to detect pathogens but rely on a set of germline-encoded activating and inhibitory receptors, which jointly orchestrate NK cell activation (Lanier, 2005). Activating receptors mostly recognize pathogen- or stress-induced ligands, and inhibitory receptors primarily bind to human leukocyte antigen (HLA) class I molecules that act as self-ligands. Thus, infected cells that down-regulate self-ligands become more susceptible to NK cells in a recognition mode termed "missing self" (Karre, 1997;

Ljunggren and Karre, 1990). An inhibitory receptor that equips NK cells with the capacity to discriminate between self and non-self is the heterodimer CD94/NKG2A, which specifically binds to nonameric peptides presented by the non-classical HLA class I molecule HLA-E (Braud et al., 1998; Lee et al., 1998a, 1998b; Llano et al., 1998). Surface expression of HLA-E/peptide complexes safeguards healthy cells from NK cell attack by inhibiting NKG2A$^+$ cells, while down-regulation of HLA-E or absence of HLA-E-stabilizing peptides results in reduced inhibition, thereby promoting missing self-responses. The HLA-E-NKG2A axis hence acts as one key determinant for NK cell activity. Consequently, viruses such as human cytomegalovirus (HCMV) or hepatitis C virus (HCV) target HLA-E for immune evasion strategies, e.g., by providing viral peptides that mimic self-peptides with the aim to inhibit NKG2A-expressing NK cells (Nattermann et al., 2005; Tomasec et al., 2000).

In line with their innate anti-viral functions, NK cell numbers correlate with the decline in viral load in patients infected with SARS-CoV-2 (Witkowski et al., 2021), and NK cells can directly curtail SARS-CoV-2 replication *in vitro* (Krämer et al., 2021; Witkowski et al., 2021). Furthermore, NK cells are robustly activated in patients with acute COVID-19, and NK cell dysfunction or exhaustion is observed in patients with severe disease, suggesting that adequate activity of NK cells may be important in disease progression (Bao et al., 2021; Krämer et al., 2021; Liao et al., 2020; Maucourant et al., 2020; Mazzoni et al., 2020; Osman et al., 2020; Sahoo et al., 2021; Varchetta et al., 2021; Wilk et al., 2020, 2021; Witkowski et al., 2021; Zenarruzabeitia et al., 2021; Zheng et al., 2020). However, the molecular mechanisms that enable NK cells to recognize SARS-CoV-2-infected cells have remained unknown. Here, we report that SARS-CoV-2 encodes for a peptide that forms stable complexes with HLA-E. The HLA-E/peptide complex does not interact with NKG2A, thereby allowing NKG2A$^+$ NK cell activation in a missing self manner. We further demonstrate that NKG2A-expressing NK cells are potently activated in the periphery, as well as in the lung microenvironment, of patients with COVID-19, and that NKG2A$^+$ NK cells proficiently suppress the replication of SARS-CoV-2 *in vitro*. Based on these findings, we propose that a SARS-CoV-2-encoded peptide presented by HLA-E may serve as viral ligand abrogating inhibition of NKG2A$^+$ NK cells and enabling missing self-recognition.

## RESULTS

### SARS-CoV-2 Non-structural protein (Nsp) 13 encodes for an HLA-E-stabilizing peptide

Previous studies have demonstrated that viruses target NKG2A for immune escape strategies, for instance, by providing peptides that stabilize HLA-E on the surface of infected cells to inhibit NK cell responses (Nattermann et al., 2005; Tomasec et al., 2000). To investigate whether SARS-CoV-2 harbors possible HLA-E-binding peptides, we predicted HLA-E-binding scores of nonamers *in silico*. We benchmarked the prediction algorithm using a non-binding irrelevant peptide from HCMV phosphoprotein pp65 as negative control (pp65$_{495–503}$; NLVPMVATV; score 0.003 [nM$^{-1}$]; Figure 1A) and a well-described HLA-E-stabilizing peptide derived from HLA-C as positive control (HLA-C$_{3-11}$; VMAPRTLIL; score 1.167 [nM$^{-1}$]; Figure 1B) (Lee et al., 1998a; Llano et al., 1998). We next applied the algorithm to the ORFeome of SARS-CoV-2 (strain Wuhan-Hu-1) and identified several nonameric peptides with high predicted binding scores (Figure 1C). The top three predicted peptides were found to be encoded by Spike glycoprotein (S$_{269-277}$; YLQPRTFLL; score 0.212 [nM$^{-1}$]), Nsp6 (Nsp6$_{114–122}$; VMYASAVVL; score 0.272 [nM$^{-1}$]), and Nsp13 (Nsp13$_{232–240}$; VMPLSAPTL; score 0.717 [nM$^{-1}$]). A separate algorithm, which includes predictors of proteasomal processing, generated identical results and further underscored Nsp13$_{232–240}$ as the top candidate (Figures S1A–S1C).

We next assessed the capacity of predicted peptides to stabilize HLA-E on the surface of HLA-E-expressing cells. To this end, we incubated synthetic peptides with K562/HLA-E cells, which are engineered to express high levels of HLA-E while simultaneously lacking cell-intrinsic HLA-E-binding peptides and therefore serve as a cellular model for HLA-E surface stabilization. Peptide pulsing at saturating concentrations revealed that Nsp13$_{232–240}$ stabilized HLA-E on the cell surface to a similar degree as the well-characterized HLA-C$_{3–11}$ peptide, while pulsing with Nsp6$_{114–122}$ and S$_{269–277}$ lead to only minor stabilization (Figure 1D). In addition, we found that Nsp13$_{232–240}$ induced HLA-E stabilization at lower concentrations than HLA-C$_{3–11}$ (Figure 1E), and pulse-chase experiments demonstrated that both peptides formed HLA-E/peptide complexes of similar stability (Figure 1F).

To obtain a deeper understanding of how Nsp13$_{232–240}$ and HLA-C$_{3–11}$ could stabilize HLA-E with similar efficiency despite considerably different amino acid sequences, we performed molecular dynamics (MD) simulations, in which we modeled the interactions of peptides with HLA-E*01:03 and $\beta_2$-microglobulin. Molecular Mechanics-Generalized Born Surface Area (MM-GBSA) was employed to compute delta energy of binding ($\Delta E_b$) as an indicator of theoretical affinity, revealing that the formation of both HLA-E/HLA-C$_{3–11}$ and HLA-E/Nsp13$_{232–240}$ complexes generated higher $\Delta E_b$ than simulated complexes with the irrelevant pp65$_{495–503}$ peptide (Figure 1G). Energy decomposition analyses further illustrated that an arginine in position 5 contributed strongly to the predicted affinity of HLA-C$_{3–11}$. In contrast, a proline in position 3 combined with a leucine in position 4 were important features of the Nsp13$_{232–240}$ peptide (Figure S1D), potentially enabling its appropriate positioning within the peptide binding groove of HLA-E (Figure 1H). In line with these simulations, a cellular thermal shift assay demonstrated that Nsp13$_{232–240}$ and HLA-C$_{3–11}$ protected HLA-E better from thermal degradation than the irrelevant pp65$_{495–503}$ peptide (Figures S1E and S1F).

Taken together, binding predictions, MD simulations, and biochemical and cellular assays identified Nsp13$_{232–240}$ as a SARS-CoV-2-encoded peptide that efficiently binds to HLA-E and forms stable HLA-E/peptide complexes.

### Common cold-causing human coronaviruses do not encode for an HLA-E-stabilizing Nsp13$_{232–240}$ peptide

We next assessed whether the presence of an HLA-E-stabilizing peptide within Nsp13 is a shared feature of other human coronaviruses (HCoVs). For this, we compared SARS-CoV-2 with SARS-CoV-1 (also known as SARS-CoV) and the four common

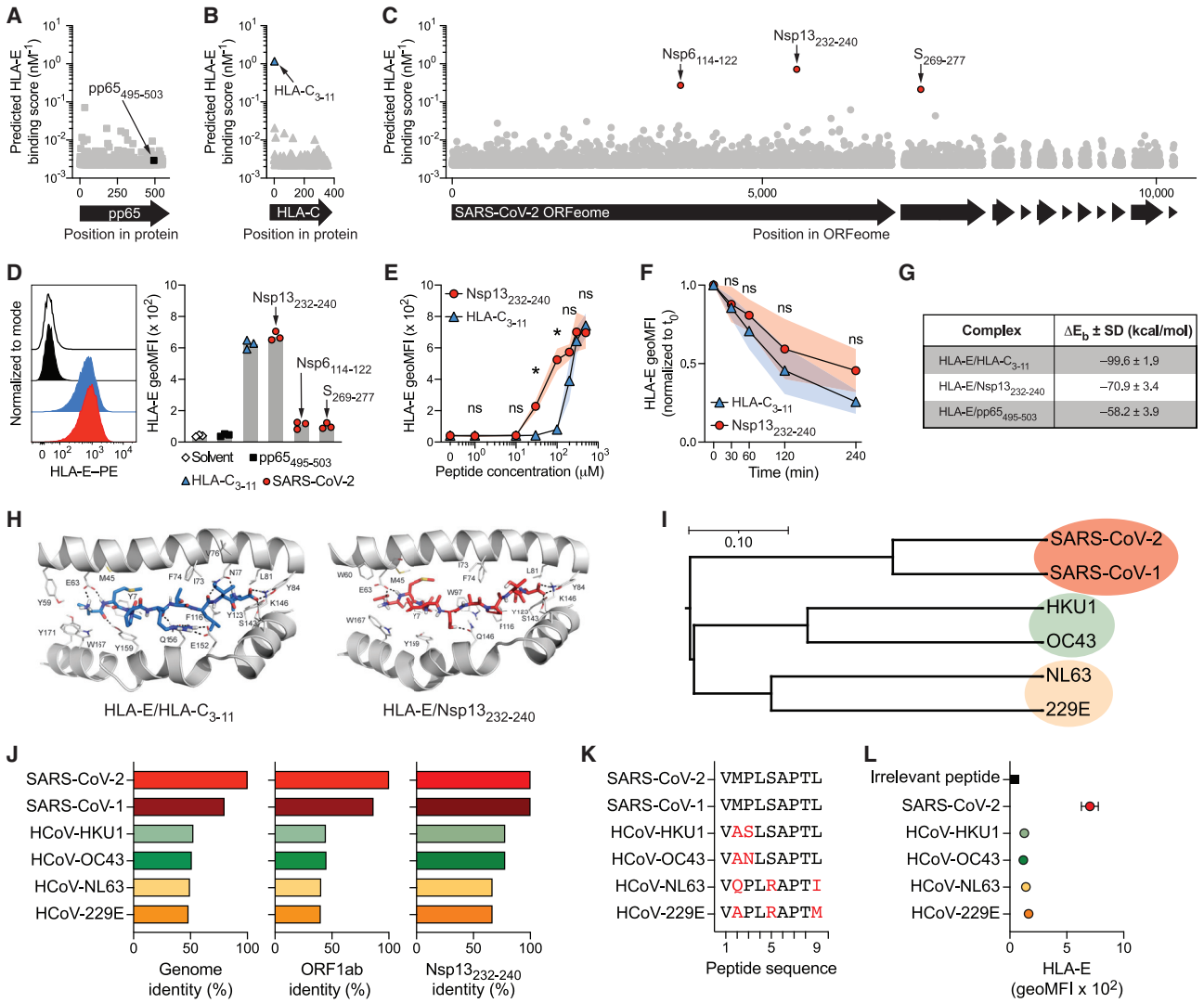


**Figure 1. SARS-CoV-2 Nsp13 encodes for an HLA-E-stabilizing peptide**

(A–C) *In silico* prediction of HLA-E*01:01-binding nonamers using NetMHC4.0. (A) pp65 protein containing the irrelevant $pp65_{495–503}$ peptide. (B) HLA-C*01:02 protein containing the known stabilizing $HLA\text{-}C_{3–11}$ peptide. (C) SARS-CoV-2 ORFeome (isolate Wuhan-Hu-1) containing the three top candidates $Nsp13_{232–240}$, $Nsp6_{114–122}$, and $S_{269–277}$.

(D) HLA-E stabilization on K562/HLA-E after pulsing with the indicated peptides at 300 μM overnight in serum-free medium. Left: representative HLA-E surface detection by flow cytometry (black line: solvent control; back filled histogram: $pp65_{495–503}$; blue filled histogram: $HLA\text{-}C_{3–11}$; red filled histogram: $Nsp13_{232–240}$). Right: summary of HLA-E stabilization as geometric mean fluorescence intensity (geoMFI; n = 3 independent experiments).

(E) HLA-E surface stabilization after peptide pulsing with varying concentrations (n = 4 independent experiments).

(F) Pulse chase of HLA-E surface levels normalized to initiation of chase ($t_0$; n = 4 independent experiments).

(G) Summary table of delta energy of binding as indicator of theoretical affinity of HLA-E/peptide complexes determined by molecular dynamics (MD) simulations (n = 3 replicate simulations).

(H) MD-based positioning of peptides in the peptide-binding groove of HLA-E. Left: $HLA\text{-}C_{3–11}$. Right: $Nsp13_{232–240}$.

(I) Phylogenetic relationships between the genomes of SARS-CoV-2, SARS-CoV-1, and common cold-causing HCoVs as determined by Clustalω. Scale bar indicates nucleotide substitution per site.

(J) Sequence identities relative to SARS-CoV-2. Left: genome level as determined by Clustalω. Middle: ORF1ab protein level as determined by Clustalω. Right: $Nsp13_{232–240}$ peptide identity.

(K) $Nsp13_{232–240}$ amino acid sequence comparison between viruses. Sequence alterations relative to SARS-CoV-2 are highlighted in red.

(L) HLA-E surface stabilization on K562/HLA-E after pulsing with $Nsp13_{232–240}$ peptides from different viruses at 300 μM overnight determined by flow cytometry and displayed as geoMFI (n = 3 independent experiments).

Data are either mean and individual data points (D) or mean ± SD (E, F, G, and L). Statistical significance was tested using two-way repeated measures ANOVA with Bonferroni correction (E and F).

*p < 0.05. See also Figure S1.

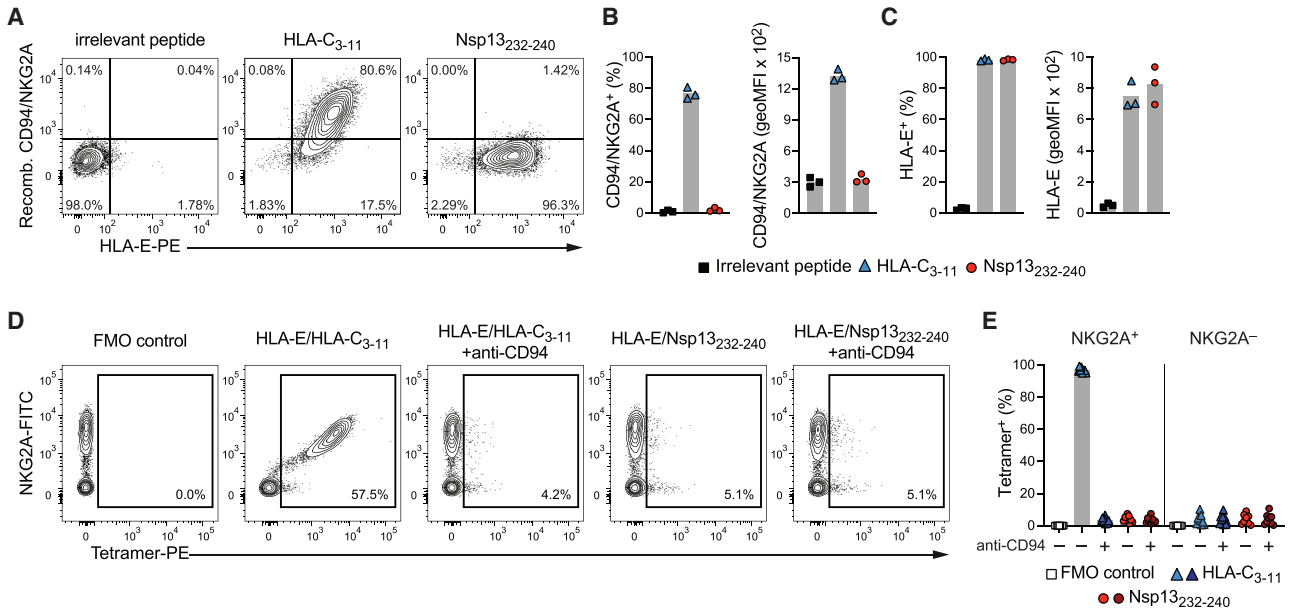


**Figure 2. HLA-E/Nsp13$_{232–240}$ complexes fail to bind to CD94/NKG2A**

(A–C) HLA-E stabilization and binding of recombinant (recomb.) CD94/NKG2A protein to K562/HLA-E after peptide pulsing at 300 μM overnight in serum-free medium. (A) Representative binding of recombinant CD94/NKG2A as determined by flow cytometry after pulsing with the indicated peptides. (B) Summaries of CD94/NKG2A binding. Left: frequency of K562/HLA-E cells positive for CD94/NKG2A. Right: degree of CD94/NKG2A bound by K562/HLA-E cells presented as geoMFI (n = 3 independent experiments). (C) Summaries of HLA-E stabilization in the same experiments. Left: frequency of K562/HLA-E cells on which HLA-E is stabilized at the cell surface. Right: degree of HLA-E surface stabilization presented as geoMFI (n = 3 independent experiments).

(D and E) Binding of HLA-E tetramers to primary CD56$^{dim}$ NKG2C$^{-}$ NK cells. (D) Representative binding of tetramers refolded with the indicated peptides in the absence or presence of blocking anti-CD94 antibodies. (E) Summary of tetramer binding to CD56$^{dim}$ NKG2C$^{-}$ NKG2A$^{+}$ and CD56$^{dim}$ NKG2C$^{-}$ NKG2A$^{-}$ NK cells without or with CD94 blockade (n = 9 donors in 3 independent experiments).

Data are mean and individual data points (B, C, and E). FMO, fluorescence minus one.

cold-causing HCoVs, namely, HKU1, OC43, 229E, and NL63 (Figure 1I). SARS-CoV-1 is highly homologous to SARS-CoV-2 and contained an identical peptide in the Nsp13$_{232–240}$ region (Figure 1J). In contrast, common cold-causing HCoVs displayed sequence alterations in two (HKU1 and OC43) or three positions (229E and NL63; Figure 1K), which resulted in noticeably lower capacity to stabilize HLA-E (Figure 1L). Further exploration of members of the sarbecovirus subgenus showed that isolates from bats and pangolins encoded Nsp13$_{232–240}$ peptides largely identical to SARS-CoV-2 (Figures S1G and S1H).

Thus, the HLA-E-stabilizing Nsp13$_{232–240}$ epitope of SARS-CoV-2 is shared by closely related sarbecoviruses but is not present in endemic common cold-causing HCoVs.

## HLA-E/Nsp13$_{232–240}$ complexes fail to bind to CD94/NKG2A

Our results thus far suggest that Nsp13$_{232–240}$ in complex with HLA-E could constitute a ligand for the NK cell receptor NKG2A. We explored potential receptor-ligand interactions by incubating recombinantly produced CD94/NKG2A heterodimers with peptide-pulsed K562/HLA-E cells to determine the degree of receptor binding to HLA-E/peptide complexes. In line with CD94/NKG2A engaging self-peptides presented by HLA-E (Braud et al., 1998; Lee et al., 1998b), we observed that cells pulsed with the HLA-C$_{3–11}$ peptide bound recombinant CD94/NKG2A at high levels. To our surprise, however, pulsing with SARS-CoV-2 Nsp13$_{232–240}$ did not result in any detectable receptor binding despite prominent surface stabilization of HLA-E (Figures 2A–2C).

As a reciprocal approach, we used HLA-E tetramers refolded with either HLA-C$_{3–11}$ or Nsp13$_{232–240}$ to assess binding of HLA-E/peptide complexes to primary NK cells. Here, HLA-E/HLA-C$_{3–11}$ tetramers were found to label nearly all NKG2A$^{+}$ CD56$^{dim}$ NK cells in a CD94-dependent manner, while the signals generated by HLA-E/Nsp13$_{232–240}$ tetramers were comparable with the negative control, independent of CD94 blockade, and similar to the staining on NKG2A$^{-}$ cells (Figures 2D and 2E).

Together, these data demonstrate that the interactions between CD94/NKG2A and HLA-E/Nsp13$_{232–240}$ are of poor quality, suggesting that HLA-E/Nsp13$_{232–240}$ complexes likely do not bind well to CD94/NKG2A receptors.

## Nsp13$_{232–240}$ presented by HLA-E unleashes NKG2A$^{+}$ NK cell activity

Given the finding that Nsp13$_{232–240}$ presented by HLA-E showed neglectable binding to recombinant CD94/NKG2A, we hypothesized that HLA-E/Nsp13$_{232–240}$ peptide complexes would render target cells susceptible to NK cell attack because of reduced inhibition of NKG2A$^{+}$ NK cells.

To test this hypothesis, we functionally interrogated the response of primary NK cells against K562/HLA-E cells presenting either the HLA-C$_{3–11}$ self-peptide, the Nsp13$_{232–240}$ virus

peptide, or the non-stabilizing $pp65_{495–503}$ irrelevant peptide. In agreement with NK cell tolerance toward self-ligands, we observed only moderate degranulation of $CD56^{dim}$ NK cells against HLA-$C_{3–11}$-pulsed target cells. In contrast, pulsing with $Nsp13_{232–240}$ resulted in elevated NK cell activity, reaching levels akin to the maximal activation elicited by the irrelevant peptide (Figures 3A and 3B).

To explore this increased susceptibility to NK cell attack in more detail, we separated NK cells expressing the HLA-E-binding activating receptor NKG2C and evaluated the contribution of NK cell sub-populations by stratifying $NKG2C^-$ $CD56^{dim}$ NK cells based on the expression of the four major inhibitory receptors, NKG2A, KIR2DL1, KIR2DL3, and KIR3DL1 (Figure S2A). Subset-level analyses demonstrated that all populations expressing NKG2A alone or in combination with other inhibitory receptors were more activated by $Nsp13_{232–240}$-pulsed than HLA-$C_{3–11}$-pulsed target cells (Figure 3C). Conversely, $NKG2A^-$ NK cell subsets were not affected by peptide pulsing, irrespective of which other inhibitory receptors were expressed (Figures 3C and S2B), indicating that differential activation was specific to $NKG2A^+$ NK cells. Accordingly, differences in the frequency of degranulation at the $CD56^{dim}$ level between $Nsp13_{232–240}$ and HLA-$C_{3–11}$ correlated with the frequency of $NKG2A^+$ NK cells present in each individual donor (Figure 3D). Moreover, effector functions of adaptive $NKG2C^+$ NK cells, which are activated by HCMV peptides in the context of HLA-E (Hammer et al., 2018a), were not triggered by $Nsp13_{232–240}$ compared with unpulsed target cells (Figure S2C). Finally, strict gating on $NKG2A^+$ $NKG2C^-$ $CD56^{dim}$ NK cells revealed complete inhibition against targets presenting the self-HLA-$C_{3–11}$ peptide and an entirely reversed response against $Nsp13_{232–240}$ with fully unleashed activation, including degranulation, expression of the cytokines tumor necrosis factor (TNF) and interferon-gamma (IFN-$\gamma$), as well as polyfunctional responses composed of all three effector functions (Figures 3E and 3F).

These results demonstrate that SARS-CoV-2 $Nsp13_{232–240}$ renders HLA-E-expressing cells susceptible to NK cell attack and underscore that the elevated NK cell activity is driven by reduced inhibition of $NKG2A^+$ cells, as such resembling missing self-recognition.

## $NKG2A^+$ NK cells are activated in patients with COVID-19 and proficiently suppress SARS-CoV-2 replication *in vitro*

Our findings indicate that $NKG2A^+$ NK cells recognize $Nsp13_{232–240}$-presenting target cells in a missing self manner. To substantiate the data obtained from *in vitro* experiments, we determined the activation profile of $NKG2A^+$ NK cells in the peripheral blood of patients with COVID-19 by expanding our previous analysis (Table S1) (Maucourant et al., 2020). In line with the robust responses that we observed *in vitro*, $NKG2A^+$ $CD56^{dim}$ NK cells from patients with COVID-19 expressed the activation marker HLA-DR and the proliferation marker Ki-67 at high frequencies *ex vivo* (Figures 4A and 4B). When directly comparing $NKG2A^-$ and $NKG2A^+$ $CD56^{dim}$ NK cells, the latter showed elevated frequencies of cells positive for HLA-DR and Ki-67 (Figure 4C), suggesting sustained activation *ex vivo*.

We further investigated NK cell responses at a local site of infection by analyzing an available single-cell RNA sequencing dataset of immune cells from bronchoalveolar lavage fluid (BALF) (Liao et al., 2020). A signature of inflammatory NK cell responses (Yang et al., 2019) clearly separated BALF NK cells of patients with COVID-19 from those of healthy controls (Figure S3A; Table S2) (Maucourant et al., 2020). The inflammatory gene set positively correlated with expression of *KLRC1* (encoding NKG2A) in NK cells from patients with COVID-19, but not in NK cells from healthy controls (Figure 4D). Among the top positively correlating transcripts were effector molecules such as *CCL5*, *GZMA*, and *GZMK*, as well as genes associated with cytoskeletal remodeling, including *CORO1A*, *TMSB4X*, and *CFL1* (Figure 4D). We captured the diversity among individual BALF NK cells from patients with COVID-19 using Uniform Manifold Approximation and Projection (UMAP) and identified six clusters (Figure 4E). We graded the clusters according to *KLRC1* expression, resulting in a $KLRC1^{low}$ bin consisting of clusters 0 and 5 and a $KLRC1^{high}$ bin containing clusters 1, 2, 3, and 4 (Figures S3B and S3C). A direct comparison between $KLRC1^{low}$ and $KLRC1^{high}$ bins demonstrated a higher score of inflammatory genes in the $KLRC1^{high}$ bin (Figure 4F), further corroborating that the $NKG2A^+$ NK cell compartment is particularly activated in patients with COVID-19.

NKG2A-expressing NK cells are present and functional in all humans, and a dimorphism in the *HLA-B* gene fine-tunes their activity by conferring slightly increased functional capacity in individuals carrying −21*M* alleles (Horowitz et al., 2016). Based on this, we explored whether −21 *HLA-B* allotypes associate with COVID-19 severity. We included 3,193 patients with COVID-19 from three described cohorts (Severe Covid-19 GWAS Group et al., 2020) in our analysis and stratified patients according to disease severity, as defined by the requirement for respiratory support (supplemental oxygen therapy or mechanical ventilation, the latter including non-invasive ventilation, invasive ventilation, and extracorporeal membrane oxygenation [ECMO]). After adjusting for confounding variables, we calculated the odds ratio (OR) of homozygous carriership of the *HLA-B* −21*M* allele with the need for respiratory support. Patients carrying the *M*/*M* genotype showed less severe disease courses in one of the cohorts (sampled in Italy; OR = 0.49; p = 0.008), no significant association was detected in the other two cohorts (sampled in Spain and Germany, respectively), and a meta-analysis of all three cohorts revealed a tendency of *M*/*M* patients for lower requirement of respiratory support (OR = 0.77; p = 0.088; Figures S3D and S3E). Thus, genetic analyses cautiously point toward a mild contribution of $NKG2A^+$ NK cells to COVID-19 severity in select cohorts.

The results obtained thus far jointly imply a role for $NKG2A^+$ NK cells in recognizing SARS-CoV-2-infected cells in a missing self manner. To directly investigate whether $NKG2A^+$ NK cells can efficiently combat the virus, we infected human A549 lung epithelial cells expressing angiotensin-converting enzyme 2 (ACE2; A549-hACE2) with SARS-CoV-2 (isolate SARS-CoV-2/human/SWE/01/2020) and co-cultured them with sorted NK cells to determine whether productive SARS-CoV-2 infection renders A549-hACE2 cells susceptible to NK cell attack, resulting in reduced viral load (Figure 4G). In line with previous reports

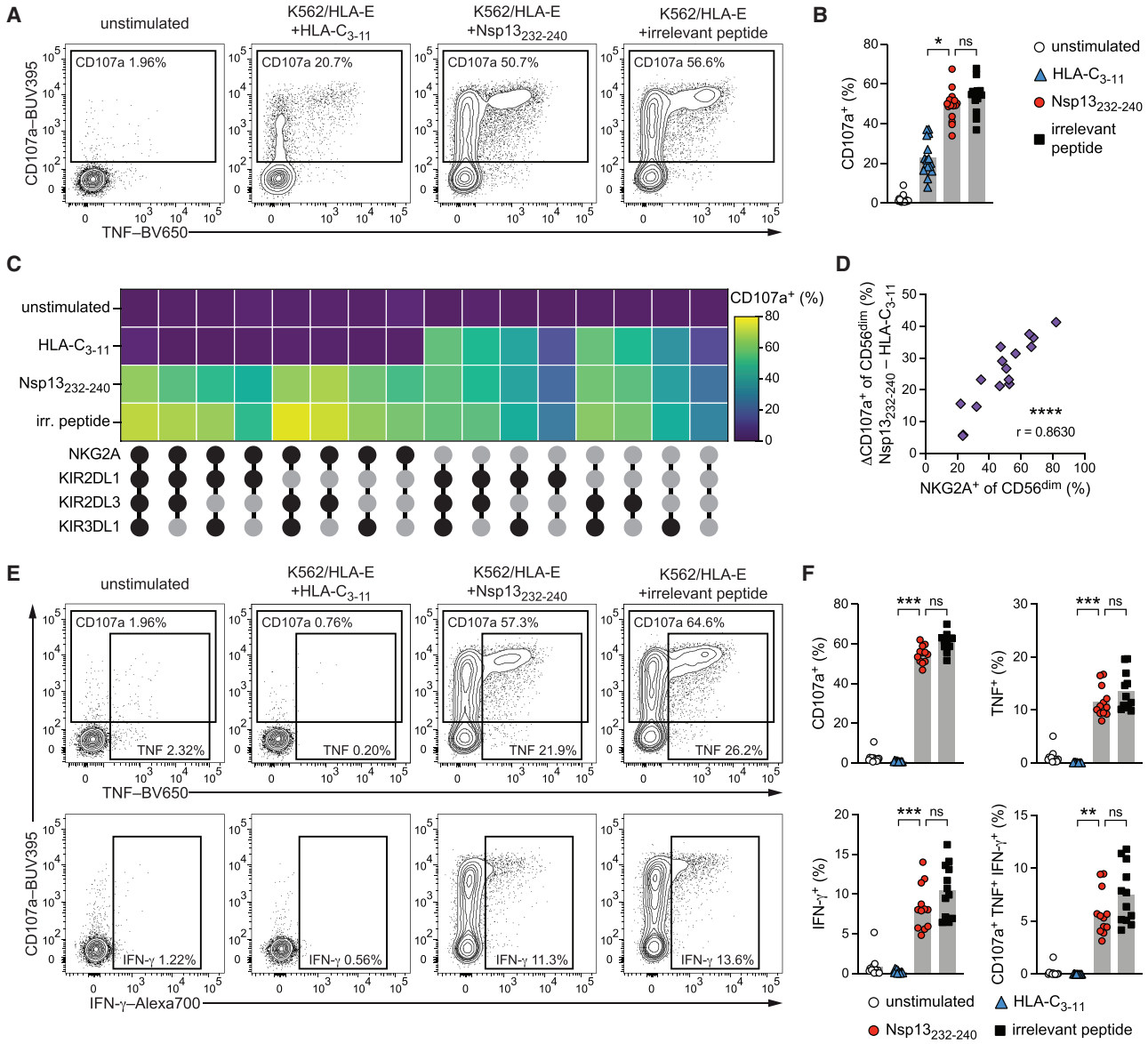


**Figure 3. $Nsp13_{232–240}$ presented by HLA-E unleashes $NKG2A^+$ NK cell activity**

NK cell activation of purified NK cells from healthy donors either left unstimulated or stimulated by co-culture with peptide-pulsed K562/HLA-E target cells as determined by flow cytometry.

(A) Representative degranulation of $CD56^{dim}$ NK cells upon co-culture with K562/HLA-E cells pulsed with the indicated peptides as measured by CD107a surface mobilization detected by flow cytometry.

(B) Summary of degranulation (n = 16 donors in 6 independent experiments).

(C) Degranulation responses of $CD56^{dim}$ $NKG2C^-$ NK cell subsets stratified for expression of NKG2A, KIR2DL1, KIR2DL3, and KIR3DL1 (black filled circle: expressed; gray filled circle: not expressed) upon co-culture with K562/HLA-E cells pulsed with the indicated peptides (n = 8 donors in 4 independent experiments).

(D) Correlation of the frequency of $NKG2A^+$ NK cells within the total $CD56^{dim}$ NK cells population and the difference in degranulation between pulsing with $Nsp13_{232–240}$ and $HLA\text{-}C_{3–11}$ (n = 16 donors in 6 independent experiments).

(E) Representative degranulation and intracellular cytokine expression of $CD56^{dim}$ $NKG2C^-$ $NKG2A^+$ NK cells upon co-culture with K562/HLA-E cells pulsed with the indicated peptides.

(F) Summaries of activation of $CD56^{dim}$ $NKG2C^-$ $NKG2A^+$ NK cells. Top left: degranulation. Top right: TNF expression. Bottom left: IFN-γ expression. Bottom right: polyfunctional ($CD107a^+$ $TNF^+$ $IFN\text{-}\gamma^+$) responses (n = 12 donors in 5 independent experiments).

Data are either mean and individual data points (B and F), mean (C), or individual data points (D). Statistical significance was tested using Friedman test with Dunn's multiple comparison test (B and F) or Spearman correlation (D). *p < 0.05, **p < 0.01, ***p < 0.001, ****p < 0.0001. irr., irrelevant. See also Figure S2.

CellPress
OPEN ACCESS

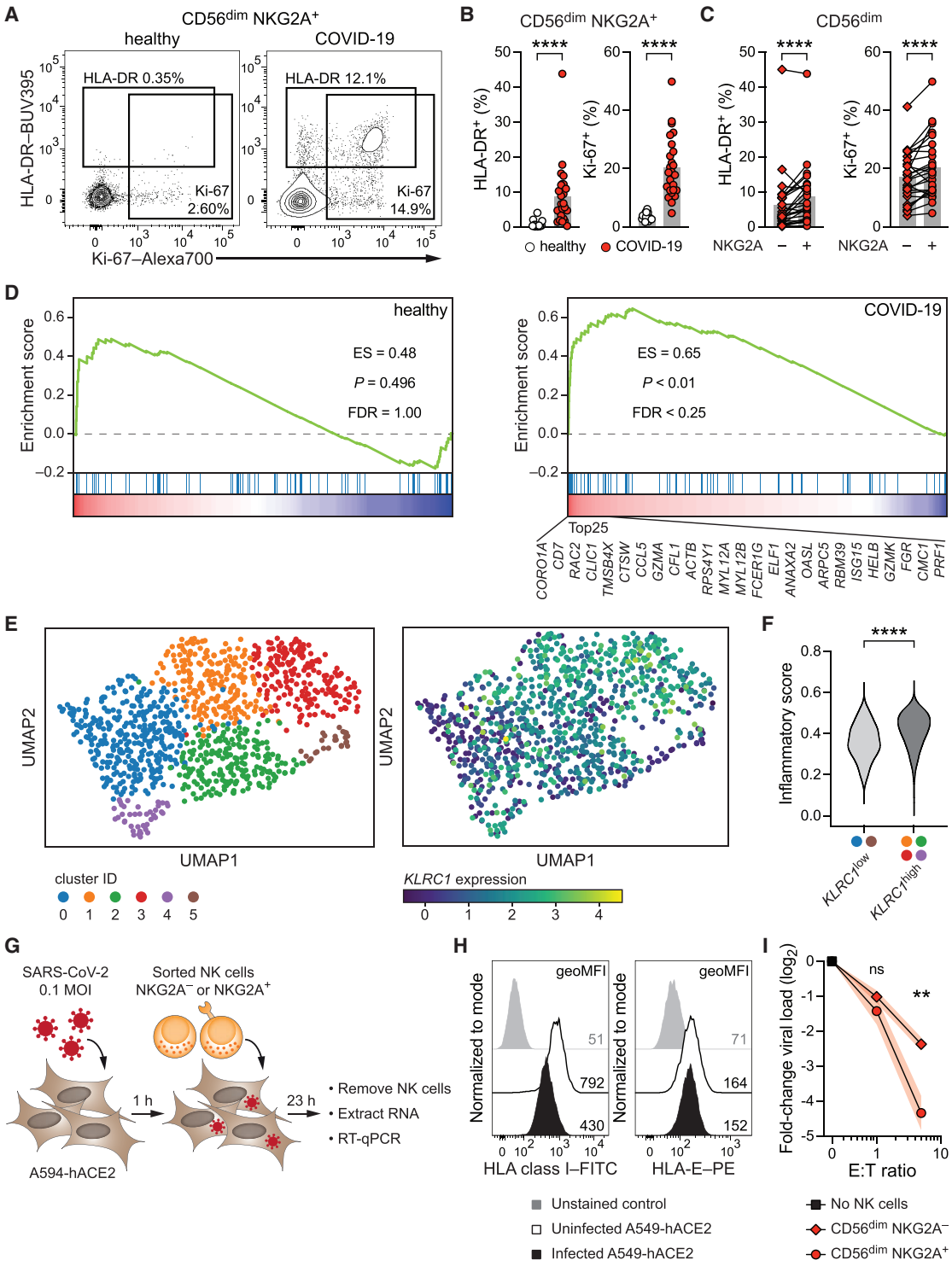


**Figure 4. NKG2A$^+$ NK cells are activated in patients with COVID-19 and proficiently suppress SARS-CoV-2 replication *in vitro***

(A–C) *Ex vivo* Activation of NKG2A$^+$ NK cells in the blood of healthy controls and of patients with COVID-19 as determined by flow cytometric detection of the activation marker HLA-DR and the proliferation marker Ki-67. (A) Representative expression of HLA-DR and Ki-67 by CD56$^{dim}$ NKG2A$^+$ NK cells. Left: healthy control. Right: patient with COVID-19. (B) Summaries of markers expressed by CD56$^{dim}$ NKG2A$^+$ NK cells in controls and patients (n = 17 healthy controls and n = 25 patients). (C) Summaries of markers expressed by NKG2A$^-$ CD56$^{dim}$ and NKG2A$^+$ CD56$^{dim}$ NK cells in patients (n = 25).

(D–F) Analysis of publicly available single-cell RNA sequencing data of *ex vivo* NK cells from BALF of healthy controls and patients with COVID-19 (Liao et al., 2020). (D) Gene set enrichment analysis (GSEA) of a signature of inflammatory responses (Table S2) (Yang et al., 2019) along with *KLRC1* expression in NK cells

*(legend continued on next page)*

indicating that SARS-CoV-2 can interfere with HLA expression (Zhang et al., 2021), we observed that classical HLA class I levels on A549-hACE2 were reduced upon infection (Figure 4H). In contrast, HLA-E surface expression was largely maintained (Figure 4H), potentially suggesting that non-HLA-A/B/C-derived peptides could be presented in this setting. Addition of sorted NKG2A$^-$ and NKG2A$^+$ CD56$^{dim}$ NK cells diminished virus copies in a dose-dependent manner (Figure S3F), akin to recent findings (Krämer et al., 2021; Witkowski et al., 2021). Strikingly, NKG2A$^+$ CD56$^{dim}$ NK cells consistently outperformed their NKG2A$^-$ counterparts in limiting viral load (Figure 4I), highlighting an enhanced capacity of NKG2A$^+$ NK cells to suppress SARS-CoV-2 replication *in vitro* despite HLA-E being present on the surface of the infected target cells.

Collectively, these data demonstrate that NKG2A$^+$ NK cells are especially activated during acute COVID-19 and exert potent anti-SARS-CoV-2 functions *in vitro*, indicating that NKG2A-expressing NK cells are not strongly inhibited by SARS-CoV-2-infected cells and may contribute to host defense against infection.

## DISCUSSION

The recognition of missing self is a functional hallmark of NK cells. Missing self-recognition is mediated by self-specific inhibitory receptors that provide tonic inhibition to NK cells when encountering healthy cells and enable robust activation through reduced inhibition against aberrant cells displaying reduced or abnormal self-ligands. Although initially postulated for recognition of tumor cells (Karre, 2008), missing self-responses are also operational in detecting infected cells and in controlling virus infections (Vidal and Lanier, 2006). In murine models of cytomegalovirus infection, missing self-recognition by NK cells expressing inhibitory Ly49 receptors contributes to virus control (Parikh et al., 2020), and virus strains that down-regulate self-ligands more strongly are attenuated *in vivo* because of facilitated missing self-recognition by NK cells (Babic et al., 2010). Furthermore, Qa-1b, the murine homologue of HLA-E, instructs antiviral responses of NKG2A$^+$ NK cells in ectromelia virus infection, during which uninfected cells display enhanced expression of Qa-1b, while infected cells down-regulate the self-ligand (Ferez et al., 2021).

NK cells display a remarkable degree of inter-individual diversity, in terms of both functionality and subset composition (Horowitz et al., 2013). Within the NK cell compartment, NKG2A is the most abundantly expressed inhibitory receptor (Fauriat et al., 2008; Horowitz et al., 2013), permitting a large fraction of NK cells to detect alterations in peptides presented by HLA-E. Interestingly, a factor that influences the frequency of NKG2A$^+$ NK cells is age: although 70% of NK cells express NKG2A in neonates, this population decreases over the life span to 30%–50% in elderly adults (Manser and Uhrberg, 2016). Reduced frequencies of NKG2A$^+$ NK cells could diminish the responder pool and potentially result in less pronounced anti-viral immunity in an age-dependent manner, paralleling reported SARS-CoV-2 fatality patterns (O'Driscoll et al., 2021).

Another factor that contributes to variability in the NK cell subset composition between individuals is HCMV serostatus. HCMV-derived peptides promote the expansion of adaptive NKG2C$^+$ NK cells (Hammer et al., 2018a), which display a composite receptor phenotype including lack of NKG2A expression (Hammer and Romagnani, 2017). Thus, HCMV-seropositive individuals, in whom adaptive NKG2C$^+$ NK cells are expanded, may possess a relatively contracted NKG2A$^+$ NK cell pool, potentially lowering the overall propensity for HLA-E-restricted missing self-responses. In line with this, the presence of adaptive NK cell populations in COVID-19 has been reported, especially in patients with severe disease (Maucourant et al., 2020; Rendeiro et al., 2020; Varchetta et al., 2021; Witkowski et al., 2021; Zenarruzabeitia et al., 2021), although HCMV seroprevalence is dependent on socioeconomic factors and age (Dowd et al., 2009), rendering the interpretation of its impact on COVID-19 severity challenging.

An immunogenetic factor that fine-tunes NK cell functionality is found within the *HLA-B* gene. A dimorphism at *HLA-B* −21 modulates HLA-E surface levels, with the −21*M* allele encoding for a peptide that stabilizes HLA-E better than the −21*T* allele (Lee et al., 1998a). Increased HLA-E stabilization by −21*M* peptides favors NKG2A$^+$ NK cell education under homeostatic conditions and enables NKG2A$^+$ NK cells to perform slightly stronger missing self-responses in −21*M*/*T* and more so −21*M*/*M* individuals (Horowitz et al., 2016). Hence although the NKG2A$^+$ compartment is also functional in individuals with *M*/*T* or *T*/*T* genotypes, we can expect NKG2A$^+$ NK cell responses to be slightly more active in individuals carrying two *M* alleles. The −21*M*/*T* dimorphism acts as indirect correlate of subtly enhanced NKG2A$^+$ NK cell function in disease settings including leukemia, where patients carrying at least one −21*M* allele showed improved outcomes after NK cell-stimulating immunotherapy (Hallner et al., 2019). Our analyses cautiously suggest that

from BALF. Left: healthy controls. Right: patients with COVID-19. The top 25 transcripts positively correlating with *KLRC1* in BALF NK cells of patients with COVID-19 are depicted. (E) UMAP plot illustrating the distribution of BALF NK cells from patients with COVID-19. Left: colored according to Leiden clustering. Right: colored based on *KLRC1* expression. (F) Inflammatory score expression between cells of the *KLRC1*$^{low}$ bin and the *KLRC1*$^{high}$ bin.

(G–I) A549-hACE2 human lung epithelial cells were infected with SARS-CoV-2 (isolate SARS-CoV-2/human/SWE/01/2020) at MOI = 0.1 and co-cultured with NK cells. (G) Schematic illustration of experimental setup. (H) Uninfected and SARS-CoV-2-infected A549-hACE2 cultured without NK cells were assessed for HLA surface expression by flow cytometry at 24 h post-infection. Left: HLA class. Right: HLA-E (representative results of two independent experiments). (I) A549-hACE2 were infected with SARS-CoV-2, followed by co-culture with sorted CD56$^{dim}$ NKG2A$^-$ and NKG2A$^+$ NK cells at the indicated effector/target (E:T) ratios starting at 1 h post-infection as in (G). Virus copies in adherent A549-hACE2 cells were quantified at 24 h post-infection by RNA isolation and RT-qPCR using the CDC nCoV-2019 N1 assay. Data are expressed as fold-change to SARS-CoV-2-infected A549-hACE cultured without NK cells (n = 6 NK cell donors in 2 independent experiments).

Data are represented as mean and individual data points (B and C), distribution (F), or mean ± SEM (I). Statistical significance was tested using Mann-Whitney *U* test (B and C), Wilcoxon signed-rank test (F), or two-way repeated measures ANOVA with Bonferroni correction (I). **p < 0.01, ****p < 0.0001.

See also Figure S3 and Tables S1 and S2.

−21*M/M* patients might be less likely to progress into severe respiratory failure, potentially because of heightened functional capacity of NKG2A$^+$ NK cells in these patients. Because this effect was observed in only one cohort, it can be safely assumed that additional genetic or environmental factors contribute to COVID-19 progression. Interestingly, the cohort containing a comparably large proportion of patients requiring only non-invasive ventilation displayed a strong effect, while two cohorts that included relatively more patients with severe disease did not show significant associations. This disparity between cohorts with varying severity distribution could suggest that a certain severity may represent a point of no return, which overrides other contributors. It is important to note that the impact of the *HLA-B* −21 dimorphism on NKG2A$^+$ NK cell function is subtle (Horowitz et al., 2016). It will be important to explore in-depth how pro-inflammatory cues balance priming of NK cells versus driving them into dysfunctional states and to which degree excessive or prolonged systemic inflammation affects anti-viral immune responses of specific subsets of NK cells (Krämer et al., 2021; Mazzoni et al., 2020; Osman et al., 2020; Sahoo et al., 2021; Wilk et al., 2021; Zheng et al., 2020).

In addition to killing of susceptible targets, NK cell effector functions include secretion of cytokines such as TNF and IFN-γ. Intriguingly, NK cells release cytokines in a non-polarized fashion (Reefman et al., 2010), which supplies cytokine signals not only to the target cell but relays them to the surrounding environment. In this manner, NK cell-derived IFN-γ can set bystander cells into anti-viral states (Schroder et al., 2004). Alerting surrounding cells is especially important at local sites of infection to limit viral replication at early time points. Because the majority of tissue-resident NK cells in human lungs display a CD56$^{bright}$ NKG2A$^+$ phenotype (Marquardt et al., 2019), it is tempting to speculate that NKG2A-expressing tissue-resident NK cells could contribute to surveillance of peptides presented by HLA-E in the lung environment and participate in combating respiratory infections *in situ*. In support of this framework, we found that NKG2A expression correlated with a signature of inflammatory responses in BALF NK cells from patients with COVID-19, indicating that NKG2A$^+$ NK cells could provide immediate anti-viral reactivity and deploy their potent suppressive functions to limit SARS-CoV-2 replication in the lung microenvironment.

Peptide-dependent recognition of virus-infected cells by inhibitory NK cell receptors has been described for pathogens that are well adapted to the human host. As such, human immunodeficiency virus (HIV)-derived peptides are presented by various HLA class I molecules and affect the binding of NK cell receptors, including NKG2A, KIR2DL2, or KIR2DL3 (Alter et al., 2011; Davis et al., 2016; Holzemer et al., 2015). Intriguingly, HIV strains encoding peptides that disrupt inhibitory interactions of HLA-C with KIR2DL2 and KIR2DL3 are underrepresented at the population level, whereas strains that encode for variants with enhanced binding are enriched, corroborating viral adaption to evade missing self-recognition (Alter et al., 2011; Holzemer et al., 2015). Similar results have been obtained for HCV, where peptide variants are selected for strong KIR2DL2 binding to inhibit NK cells (Lunemann et al., 2016). In this context, it may seem counterintuitive that SARS-CoV-2 encodes for an HLA-E-binding peptide that elicits NK cell activation by reducing inhibition. NK cell-mediated immune pressure on virus ligands (Hammer et al., 2018b) implies that the Nsp13$_{232–240}$ epitope is a likely candidate for viral evolution with selection pressure favoring an inhibitory peptide or a sequence that does not stabilize HLA-E, similar to those found in common cold-causing HCoVs. In contrast, Nsp13 possesses helicase activity and represents an essential part of the replication and transcription complex of SARS-CoV-2 (V'Kovski et al., 2021), suggesting that only mutations that do not impair viral replication are probable to emerge. Thus, closely monitoring viral evolution and functionally interrogating whether emerging SARS-CoV-2 variants harbor mutations that affect innate defense mechanisms, such as the Nsp13$_{232–240}$ epitope, will serve as a valuable source to improve our understanding of host-pathogen interactions between NK cells and SARS-CoV-2.

In summary, we show that SARS-CoV-2 Nsp13$_{232–240}$ presented by HLA-E abrogates inhibition of NKG2A$^+$ NK cells. Our data reveal that HLA-E/Nsp13$_{232–240}$ complexes are formed efficiently but fail to engage NKG2A, thereby enabling unleashed NKG2A$^+$ NK cell effector functions by missing self-recognition. In this scenario, missing self-recognition is not caused by absence of HLA-E on the cell surface but is dependent on an HLA-E-binding, viral peptide that modulates the ligand-receptor interaction toward reduced inhibition. Down-regulation of classical HLA class I during SARS-CoV-2 infection might provide a window of opportunity and favor presentation of the Nsp13$_{232–240}$ peptide on HLA-E. We thus propose that NK cells could sense a shift in the HLA-E peptide repertoire from self-peptides to a virus peptide and in such a way could utilize NKG2A as an innate recognition module to detect SARS-CoV-2-infected cells.

## Limitations of the study

In this study, we have thoroughly investigated the effect of synthetic peptides on the NK cell response. Although we used an algorithm that includes predictions of certain aspects of processing, future studies including eluting peptides from HLA-E will provide additional information on the processing of the Nsp13 protein and to which degree the Nsp13$_{232–240}$ peptide is presented by HLA-E. A caveat of such approaches may lie in the challenge to fully recapitulate proteinases (either from the host cell or encoded by SARS-CoV-2) that might be required for proper processing. Another potential limitation is that the data obtained from patients with COVID-19 discussed here are interpreted predominantly in the context of virus recognition. Our data demonstrate that in an *in vitro* environment, NKG2A$^+$ NK cells remained tolerant to self. However, it cannot be fully excluded that excessive NK cell activation may exacerbate inflammation and drive pathology, especially when considering the complex matter of COVID-19 progression.

## CONSORTIA

The members of the Karolinska COVID-19 Study Group are Mira Akber, Soo Aleman, Lena Berglin, Helena Bergsten, Niklas K. Björkström, Susanna Brighenti, Demi Brownlie, Marcus Buggert, Marta Butrym, Benedict J. Chambers, Puran Chen, Martin

Cornillet, Angelica Cuapio, Isabel Diaz Lozano, Lena Dillner, Therese Djärv, Majda Dzidic, Johanna Emgård, Lars I. Eriksson, Malin Flodström-Tullberg, Hedvig Glans, Jean-Baptiste Gorin, Sara Gredmark-Russ, Jonathan Grip, Quirin Hammer, Alvaro Haroun-Izquierdo, Elisabeth Henriksson, Laura Hertwig, Sadaf Kalsum, Tobias Kammann, Jonas Klingström, Efthymia Kokkinou, Egle Kvedaraite, Hans-Gustaf Ljunggren, Marco Giulio Loreti, Magdalini Lourda, Kimia T. Maleki, Karl-Johan Malmberg, Nicole Marquardt, Johan Mårtensson, Christopher Maucourant, Jakob Michaëlsson, Jenny Mjösberg, Kirsten Moll, Jagadeeswara Rao Muvva, Pontus Nauclér, Anna Norrby-Teglund, Laura M. Palma Medina, Tiphaine Parrot, André Perez-Potti, Björn P. Persson, Lena Radler, Dorota Religa, Emma Ringqvist, Olga Rivera-Ballesteros, Olav Rooyackers, Johan K. Sandberg, John Tyler Sandberg, Takuya Sekine, Ebba Sohlberg, Tea Soini, Anders Sönnerborg, Kristoffer Strålin, Benedikt Strunz, Mattias Svensson, Janne Tynell, Christian Unge, Renata Varnaite, Andreas von Kries, and David Wulliman.

The members of the Severe COVID-19 GWAS group are Aaron Blandino Ortiz, Adolfo de Salazar, Adolfo Garrido Chercoles, Adriana Palom, Agustín Albillos, Agustín Ruiz, Alba-Estela Garcia-Fernandez, Albert Blanco-Grau, Alberto Mantovani, Alberto Zanella, Aleksander Rygh Holten, Alena Mayer, Alessandra Bandera, Alessandro Cherubini, Alessandro Protti, Alessio Aghemo, Alessio Gerussi, Alexander Popov, Alfredo Ramirez, Alice Braun, Almut Nebel, Ana Barreira, Ana Lleo, Ana Teles, Anders Benjamin Kildal, Andre Franke, Andrea Biondi, Andrea Caballero-Garralda, Andrea Ganna, Andrea Gori, Andreas Glück, Andreas Lind, Anja Tanck, Anke Hinney, Anna Carreras Nolla, Anna Latiano, Anna Ludovica Fracanzani, Anna Peschuck, Annalisa Cavallero, Anne Ma Dyrhol-Riise, Antonella Ruello, Antonio Julià, Antonio Muscatello, Antonio Pesenti, Antonio Voza, Ariadna Rando-Segura, Aurora Solier, Beatriz Cortes, Beatriz Mateos, Beatriz Nafria-Jimenez, Benedikt Schaefer, Bettina Heidecker, Björn Jensen, Carla Bellinghausen, Carlo Maj, Carlos Ferrando, Carmen de la Horra, Carmen Quereda, Carsten Skurk, Charlotte Thibeault, Chiara Scollo, Christian Herr, Christoph D. Spinner, Christoph Gassner, Christoph Lange, Cinzia Hu, Cinzia Paccapelo, Clara Lehmann, Claudio Angelini, Claudio Cappadona, Clinton Azuure, Cristiana Bianco, Cristina Cea, Cristina Sancho, Dag Arne Lihaug Hoff, Daniela Galimberti, Daniele Prati, David Ellinghaus, David Haschka, David Jiménez, David Pestaña, David Toapanta, Douglas Maya-Miles, Eduardo Muñiz-Diaz, Eike M. Wacker, Elena Azzolini, Elena Sandoval, Eleonora Binatti, Elio Scarpini, Elisa T. Helbig, Eloisa Urrechaga, Elvezia Maria Paraboschi, Emanuele Pontali, Enric Reverter, Enrique J. Calderón, Enrique Navas, Erik Solligård, Ernesto Contro, Eunate Arana, Eva C. Schulte, Fátima Aziz, Federico Garcia, Félix García Sánchez, Ferruccio Ceriotti, Filippo Martinelli-Boneschi, Flora Peyvandi, Florian Kurth, Florian Tran, Florian Uellendahl-Werth, Francesco Blasi, Francesco Malvestiti, Francisco J. Medrano, Francisco Mesonero, Francisco Rodriguez-Frias, Frank Hanses, Frauke Degenhardt, Fredrik Müller, Georg Hemmrich-Stanisak, Giacomo Bellani, Giacomo Grasselli, Gianni Pezzoli, Giorgio Costantino, Giovanni Albano, Giulia Cardamone, Giuseppe Bellelli, Giuseppe Citerio, Giuseppe Foti, Giuseppe Lamorte, Giuseppe Matullo, Guido Baselli, Hayato Kurihara, Heinz Zoller, Hesham ElAbd, Holger Neb, Ilaria My, Ingo Kurth, Isabel Hernández, Isabell Pink, Itziar de Rojas, Iván Galván-Femenia, Jan C. Holter, Jan Egil Afset, Jan Heyckendorf, Jan Kässens, Jan Kristian Damås, Jan Rybniker, Janine Altmüller, Jatin Arora, Javier Ampuero, Javier Fernández, Javier Martín, Jeanette Erdmann, Jesus M. Banales, Joan Ramon Badia, Joaquin Dopazo, Jochen Schneider, Johannes R. Hov, Jon Lerga-Jaso, Jonas Bergan, Jordi Barretina, Jörn Walter, Jose Hernández Quero, Josune Goikoetxea, Juan Delgado, Juan M. Guerrero, Julia Fazaal, Julia Kraft, Julia Schröder, Kari Risnes, Karina Banasik, Karl Erik Müller, Karoline I. Gaede, Kerstin U. Ludwig, Koldo Garcia-Etxebarria, Kristian Tonby, Lars Heggelund, Lars Wienbrandt, Laura Izquierdo-Sanchez, Laura Rachele Bettini, Lauro Sumoy, Leif Erik Sander, Lena J. Lippert, Leonardo Terranova, Lindokuhle Nkambule, Lisa Knopp, Lise Tuset Gustad, Luca Valenti, Lucia Garbarino, Luigi Santoro, Luigia Scudeller, Luis Bujanda, Luis Téllez, Luisa Roade, Mahnoosh Ostadreza, Maider Intxausti, Malte C. Rühlemann, Manolis Kogevinas on behalf of the COVICAT study group, Manuel Romero-Gómez, Mar Riveiro-Barciela, Marc M. Berger, Marco Schaefer, Mareike Wendorff, Mari E.K. Niemi, María A. Gutiérrez-Stampa, Maria Buti, Maria Carrabba, Maria E. Figuera Basso, Maria Grazia Valsecchi, María Hernandez-Tejero, Maria J.G.T. Vehreschild, Maria Manunta, Marialbert Acosta-Herrera, Mariella D'Angiò, Marina Baldini, Marina Cazzaniga, Mario Cáceres, Marit M. Grimsrud, Markus Cornberg, Markus M. Nöthen, Marta Marquié, Massimo Castoldi, Mattia Cordioli, Maurizio Cecconi, Mauro D'Amato, Max Augustin, May Sissel Vadla, Melissa Tomasi, Mercè Boada, Michael Dreher, Michael J. Seilmaier, Michael Joannidis, Michael Wittig, Michela Mazzocco, Michele Ciccarelli, Miguel Rodríguez-Gandía, Monica Bocciolone, Monica Miozzo, Natale Imaz Ayo, Natalia Blay, Natalia Chueca, Nicola Montano, Nicole Braun, Nicole Ludwig, Nikolaus Marx, Nilda Martínez, Ole Bernt Lenning, Oliver A. Cornely, Oliver Witzke, Onur Özer, Orazio Palmieri, Paola Faverio, Paoletta Preatoni, Paolo Bonfanti Paolo Omodei, Paolo Tentorio, Pedro Castro, Pedro M. Rodrigues, Pedro Pablo España, Per Hoffmann, Petra Bacher, Philip Rosenstiel, Philipp Koehler, Philipp Schommers, Phillip Suwalski, Pietro Invernizzi, Rafael de Cid on behalf of the COVICAT study group, Raúl de Pablo, Ricard Ferrer, Robert Bals, Roberta Gualtierotti, Rocío Gallego-Durán, Ronny Myhre, Rosa Nieto, Rosanna Asselta, Rossana Carpani, Rubén Morilla, Salvatore Badalamenti, Sammra Haider, Sandra Ciesek, Sandra May, Sara Bombace, Sara Marsal, Sara Pigazzini, Sebastian Klein, Selina Rolker, Serena Aneli, Serena Pelusi, Sibylle Wilfling, Siegfried Goerg, Silvano Bosari, Simonas Juzenas, Søren Brunak, Soumya Raychaudhuri, Stefan Schreiber, Stefanie Heilmann-Heimbach, Stefano Aliberti, Stefano Duga, Stephan Ripke, Susanne Dudman, Tanja Wesse, Tenghao Zheng, Thomas Bahmer, Thomas Eggermann, Thomas Illig, Thorsten Brenner, Tobias L. Lenz, Tom H. Karlsen, Tomas Pumarola, Torsten Feldt, Trine Folseraas, Trinidad Gonzalez Cejudo, Ulf Landmesser, Ulrike Protzer, Ute Hehr, Valeria Rimoldi, Valter Monzani, Vegard Skogen, Verena Keitel, Verena Kopfnagel, Vicente Friaza, Victor Andrade, Victor Moreno, Wolfgang Albrecht, Wolfgang Peter, Wolfgang Poller, Xavier Farre, Xiaoli Yi, Xiaomin Wang, Ximo Dopazo, Yascha Khodamoradi, Zehra Karadeniz, COVICAT study group, Covid-19 Aachen Study (COVAS), Pa COVID-19 Study Group, The Humanitas COVID-19 Task Force, and The Humanitas Gavazzeni COVID-19 Task Force.

## STAR★METHODS

Detailed methods are provided in the online version of this paper and include the following:

- KEY RESOURCES TABLE
- RESOURCE AVAILABILITY
  - Lead contact
  - Materials availability
  - Data and code availability
- EXPERIMENTAL MODEL AND SUBJECT DETAILS
  - Human subjects
  - Culture conditions for *in vitro* systems
  - Cell lines
- METHOD DETAILS
  - HLA-E binding prediction
  - HLA-E surface stabilization
  - Flow cytometry
  - Molecular dynamics simulations
  - Phylogenetic analyses
  - Cellular thermal shift assay
  - HLA-E tetramers
  - Functional assays
  - Re-analysis of NK cell activation in a previously described patient cohort
  - Re-analysis of NK cell activity in a previously reported single-cell RNA sequencing dataset
  - Genetic association analysis of *HLA-B –21*
  - Virus inhibition assay
- QUANTIFICATION AND STATISTICAL ANALYSIS

## SUPPLEMENTAL INFORMATION

Supplemental information can be found online at https://doi.org/10.1016/j.celrep.2022.110503.

## ACKNOWLEDGMENTS

We thank the NIH Tetramer Core Facility for providing HLA-E tetramers, as well as Alba Corman, Bartlomiej Porebski, and Oscar Fernandez-Capetillo (all Karolinska Institute) for kindly sharing A549-hACE2. We thank Silje Krokeide for assistance and Johnna Olweus, Fridtjof Lund-Johansen, and Tom Hemming Karlsen (all Oslo University Hospital) for feedback critical to the development of the project. We are grateful to all members of the Malmberg lab and the Center for Infectious Medicine for inspiring discussions.

This study has received funding from the European Union's Horizon 2020 research and innovation program under Marie Skłodowska-Curie grant agreement no. 838909 (Q.H.). J.D. was supported by German Research Foundation grant DU1964/1-1. H.-G.L. and the Karolinska COVID-19 Study Group were supported by Knut and Alice Wallenberg Foundation and Nordstjernan AB. Support for this work was provided by the Karolinska Institute Foundation for Virus Research grant 2021-00069 (Q.H.), Hedlunds Foundations grant M2021-1533 (Q.H.), Clas Groschinskys Foundation grant M21120 (Q.H.), Lars Hiertas Minne Foundation grant FO2021-0263 (Q.H.), the Tornspiran Foundation (Q.H.), South-Eastern Norway Regional Health Authority grant 2021073 (K.-J.M.), Norwegian Cancer Society grant 223310 (K.-J.M.), Research Council of Norway grant 275469 (K.-J.M.), Swedish Childhood Cancer Fund grant PR2020-0159 (K.-J.M.), Swedish Cancer Society grant CAN 2017/676 (K.-J.M.), Knut and Alice Wallenberg Foundation grant KAW 2018-011 (K.-J.M.), and Swedish Research Council grant 2020-02286 (K.-J.M.).

## AUTHOR CONTRIBUTIONS

Conceptualization: Q.H., J.D., K.-J.M.; methodology: Q.H., J.D., W.C., F.P.; investigation: Q.H., J.D., W.C., F.P., P.M., O.H., H.K.N., K.T.M., M.G., T.S., F.S., M.M., J.K.; formal analysis: M.W., F.D.; resources: E.S., V.A., M.A., A.F., J.M., N.K.B., T.R., C.R., A.H., J.K., H.-G.L.; writing – original draft: Q.H.; writing – review & editing: all authors; supervision: Q.H., K.-J.M.; project administration: Q.H., K.-J.M.; funding acquisition: Q.H., K.-J.M.

## DECLARATION OF INTERESTS

H.-G.L. is a member of the Board of XNK Therapeutics AB and Vycellix Inc. K.-J.M. is a Scientific Advisor and has a research grant from Fate Therapeutics and is a member of the Scientific Advisory Board of Vycellix Inc. The other authors declare no competing interests.

Received: October 12, 2021
Revised: January 12, 2022
Accepted: February 15, 2022
Published: February 21, 2022

## REFERENCES

Alter, G., Heckerman, D., Schneidewind, A., Fadda, L., Kadie, C.M., Carlson, J.M., Oniangue-Ndza, C., Martin, M., Li, B., Khakoo, S.I., et al. (2011). HIV-1 adaptation to NK-cell-mediated immune pressure. Nature *476*, 96–100. https://doi.org/10.1038/nature10237.

Andreatta, M., and Nielsen, M. (2016). Gapped sequence alignment using artificial neural networks: application to the MHC class I system. Bioinformatics *32*, 511–517. https://doi.org/10.1093/bioinformatics/btv639.

Babic, M., Pyzik, M., Zafirova, B., Mitrovic, M., Butorac, V., Lanier, L.L., Krmpotic, A., Vidal, S.M., and Jonjic, S. (2010). Cytomegalovirus immunoevasin reveals the physiological role of "missing self" recognition in natural killer cell dependent virus control *in vivo*. J. Exp. Med. *207*, 2663–2673. https://doi.org/10.1084/jem.20100921.

Bao, C., Tao, X., Cui, W., Hao, Y., Zheng, S., Yi, B., Pan, T., Young, K.H., and Qian, W. (2021). Natural killer cells associated with SARS-CoV-2 viral RNA shedding, antibody response and mortality in COVID-19 patients. Exp. Hematol. Oncol. *10*, 5. https://doi.org/10.1186/s40164-021-00199-1.

Berman, H.M., Westbrook, J., Feng, Z., Gilliland, G., Bhat, T.N., Weissig, H., Shindyalov, I.N., and Bourne, P.E. (2000). The protein Data Bank. Nucleic Acids Res. *28*, 235–242. https://doi.org/10.1093/nar/28.1.235.

Bjorkstrom, N.K., Strunz, B., and Ljunggren, H.G. (2021). Natural killer cells in antiviral immunity. Nat. Rev. Immunol. *22*, 112–123. https://doi.org/10.1038/s41577-021-00558-3.

Braud, V.M., Allan, D.S., O'Callaghan, C.A., Soderstrom, K., D'Andrea, A., Ogg, G.S., Lazetic, S., Young, N.T., Bell, J.I., Phillips, J.H., et al. (1998). HLA-E binds to natural killer cell receptors CD94/NKG2A, B and C. Nature *391*, 795–799. https://doi.org/10.1038/35869.

Case, D.A., Cheatham, T.E., 3rd, Darden, T., Gohlke, H., Luo, R., Merz, K.M., Jr., Onufriev, A., Simmerling, C., Wang, B., and Woods, R.J. (2005). The Amber biomolecular simulation programs. J. Comput. Chem. *26*, 1668–1688. https://doi.org/10.1002/jcc.20290.

Cossarizza, A., Chang, H.D., Radbruch, A., Akdis, M., Andra, I., Annunziato, F., Bacher, P., Barnaba, V., Battistini, L., Bauer, W.M., et al. (2017). Guidelines for the use of flow cytometry and cell sorting in immunological studies. Eur. J. Immunol. *47*, 1584–1797. https://doi.org/10.1002/eji.201646632.

Davis, Z.B., Cogswell, A., Scott, H., Mertsching, A., Boucau, J., Wambua, D., Le Gall, S., Planelles, V., Campbell, K.S., and Barker, E. (2016). A conserved HIV-1-Derived peptide presented by HLA-E renders infected T-cells highly susceptible to attack by NKG2A/CD94-bearing natural killer cells. PLoS Pathog. *12*, e1005421. https://doi.org/10.1371/journal.ppat.1005421.

Degenhardt, F., Ellinghaus, D., Juzenas, S., Lerga-Jaso, J., Wendorff, M., Maya-Miles, D., Uellendahl-Werth, F., ElAbd, H., Arora, J., Özer, O., et al. (2021). New susceptibility loci for severe COVID-19 by detailed GWAS analysis

in European populations. Preprint at medRxiv. https://doi.org/10.1101/2021.07.21.21260624.

Dowd, J.B., Aiello, A.E., and Alley, D.E. (2009). Socioeconomic disparities in the seroprevalence of cytomegalovirus infection in the US population: NHANES III. Epidemiol. Infect. *137*, 58–65. https://doi.org/10.1017/S0950268808000551.

Fauriat, C., Andersson, S., Bjorklund, A.T., Carlsten, M., Schaffer, M., Bjorkstrom, N.K., Baumann, B.C., Michaelsson, J., Ljunggren, H.G., and Malmberg, K.J. (2008). Estimation of the size of the alloreactive NK cell repertoire: studies in individuals homozygous for the group A KIR haplotype. J. Immunol. *181*, 6010–6019. https://doi.org/10.4049/jimmunol.181.9.6010.

Ferez, M., Knudson, C.J., Lev, A., Wong, E.B., Alves-Peixoto, P., Tang, L., Stotesbury, C., and Sigal, L.J. (2021). Viral infection modulates Qa-1b in infected and bystander cells to properly direct NK cell killing. J. Exp. Med. *218*, e20201782. https://doi.org/10.1084/jem.20201782.

Guan, W.J., Ni, Z.Y., Hu, Y., Liang, W.H., Ou, C.Q., He, J.X., Liu, L., Shan, H., Lei, C.L., Hui, D.S.C., et al. (2020). Clinical characteristics of coronavirus disease 2019 in China. New Engl. J. Med. *382*, 1708–1720. https://doi.org/10.1056/NEJMoa2002032.

Hallner, A., Bernson, E., Hussein, B.A., Ewald Sander, F., Brune, M., Aurelius, J., Martner, A., Hellstrand, K., and Thoren, F.B. (2019). The HLA-B -21 dimorphism impacts on NK cell education and clinical outcome of immunotherapy in acute myeloid leukemia. Blood *133*, 1479–1488. https://doi.org/10.1182/blood-2018-09-874990.

Hammer, Q., and Romagnani, C. (2017). About training and memory: NK-cell adaptation to viral infections. Adv. Immunol. *133*, 171–207. https://doi.org/10.1016/bs.ai.2016.10.001.

Hammer, Q., Ruckert, T., Borst, E.M., Dunst, J., Haubner, A., Durek, P., Heinrich, F., Gasparoni, G., Babic, M., Tomic, A., et al. (2018a). Peptide-specific recognition of human cytomegalovirus strains controls adaptive natural killer cells. Nat. Immunol. *19*, 453–463. https://doi.org/10.1038/s41590-018-0082-6.

Hammer, Q., Ruckert, T., and Romagnani, C. (2018b). Natural killer cell specificity for viral infections. Nat. Immunol. *19*, 800–808. https://doi.org/10.1038/s41590-018-0163-6.

Holzemer, A., Thobakgale, C.F., Jimenez Cruz, C.A., Garcia-Beltran, W.F., Carlson, J.M., van Teijlingen, N.H., Mann, J.K., Jaggernath, M., Kang, S.G., Korner, C., et al. (2015). Selection of an HLA-C*03:04-Restricted HIV-1 p24 gag sequence variant is associated with viral escape from KIR2DL3+ natural killer cells: data from an observational cohort in South Africa. PLoS Med. *12*, e1001900, discussion e1001900. https://doi.org/10.1371/journal.pmed.1001900.

Horowitz, A., Djaoud, Z., Nemat-Gorgani, N., Blokhuis, J., Hilton, H.G., Beziat, V., Malmberg, K.J., Norman, P.J., Guethlein, L.A., and Parham, P. (2016). Class I HLA haplotypes form two schools that educate NK cells in different ways. Sci. Immunol. *1*, eaag1672. https://doi.org/10.1126/sciimmunol.aag1672.

Horowitz, A., Strauss-Albee, D.M., Leipold, M., Kubo, J., Nemat-Gorgani, N., Dogan, O.C., Dekker, C.L., Mackey, S., Maecker, H., Swan, G.E., et al. (2013). Genetic and environmental determinants of human NK cell diversity revealed by mass cytometry. Sci. translational Med. *5*, 208ra145. https://doi.org/10.1126/scitranslmed.3006702.

Jacobson, M.P., Pincus, D.L., Rapp, C.S., Day, T.J., Honig, B., Shaw, D.E., and Friesner, R.A. (2004). A hierarchical approach to all-atom protein loop prediction. Proteins *55*, 351–367. https://doi.org/10.1002/prot.10613.

Karre, K. (1997). How to recognize a foreign submarine. Immunological Rev. *155*, 5–9. https://doi.org/10.1111/j.1600-065x.1997.tb00935.x.

Karre, K. (2008). Natural killer cell recognition of missing self. Nat. Immunol. *9*, 477–480. https://doi.org/10.1038/ni0508-477.

Krämer, B., Knoll, R., Bonaguro, L., ToVinh, M., Raabe, J., Astaburuaga-García, R., Schulte-Schrepping, J., Kaiser, K.M., Rieke, G.J., Bischoff, J., et al. (2021). Early IFN-α signatures and persistent dysfunction are distinguishing features of NK cells in severe COVID-19. Immunity *54*, 2650–2669.e14. https://doi.org/10.1016/j.immuni.2021.09.002.

Lanier, L.L. (2005). NK cell recognition. Annu. Rev. Immunol. *23*, 225–274. https://doi.org/10.1146/annurev.immunol.23.021704.115526.

Lee, N., Goodlett, D.R., Ishitani, A., Marquardt, H., and Geraghty, D.E. (1998a). HLA-E surface expression depends on binding of TAP-dependent peptides derived from certain HLA class I signal sequences. J. Immunol. *160*, 4951–4960.

Lee, N., Llano, M., Carretero, M., Ishitani, A., Navarro, F., Lopez-Botet, M., and Geraghty, D.E. (1998b). HLA-E is a major ligand for the natural killer inhibitory receptor CD94/NKG2A. Proc. Natl. Acad. Sci. U S A *95*, 5199–5204. https://doi.org/10.1073/pnas.95.9.5199.

Letunic, I., and Bork, P. (2021). Interactive Tree of Life (iTOL) v5: an online tool for phylogenetic tree display and annotation. Nucleic Acids Res. *49*, W293–W296. https://doi.org/10.1093/nar/gkab301.

Liao, M., Liu, Y., Yuan, J., Wen, Y., Xu, G., Zhao, J., Cheng, L., Li, J., Wang, X., Wang, F., et al. (2020). Single-cell landscape of bronchoalveolar immune cells in patients with COVID-19. Nat. Med. *26*, 842–844. https://doi.org/10.1038/s41591-020-0901-9.

Ljunggren, H.G., and Karre, K. (1990). In search of the 'missing self': MHC molecules and NK cell recognition. Immunol. Today *11*, 237–244. https://doi.org/10.1016/0167-5699(90)90097-s.

Llano, M., Lee, N., Navarro, F., Garcia, P., Albar, J.P., Geraghty, D.E., and Lopez-Botet, M. (1998). HLA-E-bound peptides influence recognition by inhibitory and triggering CD94/NKG2 receptors: preferential response to an HLA-G-derived nonamer. Eur. J. Immunol. *28*, 2854–2863. https://doi.org/10.1002/(SICI)1521-4141(199809)28:09<2854::AID-IMMU2854>3.0.CO;2-W.

Lunemann, S., Martrus, G., Holzemer, A., Chapel, A., Ziegler, M., Korner, C., Garcia Beltran, W., Carrington, M., Wedemeyer, H., and Altfeld, M. (2016). Sequence variations in HCV core-derived epitopes alter binding of KIR2DL3 to HLA-C *03:04 and modulate NK cell function. J. Hepatol. *65*, 252–258. https://doi.org/10.1016/j.jhep.2016.03.016.

Madeira, F., Park, Y.M., Lee, J., Buso, N., Gur, T., Madhusoodanan, N., Basutkar, P., Tivey, A.R.N., Potter, S.C., Finn, R.D., and Lopez, R. (2019). The EMBL-EBI search and sequence analysis tools APIs in 2019. Nucleic Acids Res. *47*, W636–W641. https://doi.org/10.1093/nar/gkz268.

Maier, J.A., Martinez, C., Kasavajhala, K., Wickstrom, L., Hauser, K.E., and Simmerling, C. (2015). ff14SB: improving the accuracy of protein side chain and backbone parameters from ff99SB. J. Chem. Theory Comput. *11*, 3696–3713. https://doi.org/10.1021/acs.jctc.5b00255.

Manser, A.R., and Uhrberg, M. (2016). Age-related changes in natural killer cell repertoires: impact on NK cell function and immune surveillance. Cancer Immunol. Immunother. *65*, 417–426. https://doi.org/10.1007/s00262-015-1750-0.

Marquardt, N., Kekalainen, E., Chen, P., Lourda, M., Wilson, J.N., Scharenberg, M., Bergman, P., Al-Ameri, M., Hard, J., Mold, J.E., et al. (2019). Unique transcriptional and protein-expression signature in human lung tissue-resident NK cells. Nat. Commun. *10*, 3841. https://doi.org/10.1038/s41467-019-11632-9.

Martinez Molina, D., Jafari, R., Ignatushchenko, M., Seki, T., Larsson, E.A., Dan, C., Sreekumar, L., Cao, Y., and Nordlund, P. (2013). Monitoring drug target engagement in cells and tissues using the cellular thermal shift assay. Science *341*, 84–87. https://doi.org/10.1126/science.1233606.

Maucourant, C., Filipovic, I., Ponzetta, A., Aleman, S., Cornillet, M., Hertwig, L., Strunz, B., Lentini, A., Reinius, B., Brownlie, D., et al. (2020). Natural killer cell immunotypes related to COVID-19 disease severity. Sci. Immunol. *5*, eabd6832. https://doi.org/10.1126/sciimmunol.abd6832.

Mazzoni, A., Salvati, L., Maggi, L., Capone, M., Vanni, A., Spinicci, M., Mencarini, J., Caporale, R., Peruzzi, B., Antonelli, A., et al. (2020). Impaired immune cell cytotoxicity in severe COVID-19 is IL-6 dependent. J. Clin. Invest. *130*, 4694–4703. https://doi.org/10.1172/JCI138554.

Miller, B.R., 3rd, McGee, T.D., Jr., Swails, J.M., Homeyer, N., Gohlke, H., and Roitberg, A.E. (2012). MMPBSA.py: an efficient program for end-state free

energy calculations. J. Chem. Theory Comput. *8*, 3314–3321. https://doi.org/10.1021/ct300418h.

Morse, C., Tabib, T., Sembrat, J., Buschur, K.L., Bittar, H.T., Valenzi, E., Jiang, Y., Kass, D.J., Gibson, K., Chen, W., et al. (2019). Proliferating SPP1/MERTK-expressing macrophages in idiopathic pulmonary fibrosis. Eur. Respir. J. *54*, 1802441. https://doi.org/10.1183/13993003.02441-2018.

Nattermann, J., Nischalke, H.D., Hofmeister, V., Ahlenstiel, G., Zimmermann, H., Leifeld, L., Weiss, E.H., Sauerbruch, T., and Spengler, U. (2005). The HLA-A2 restricted T cell epitope HCV core 35-44 stabilizes HLA-E expression and inhibits cytolysis mediated by natural killer cells. Am. J. Pathol. *166*, 443–453. https://doi.org/10.1016/S0002-9440(10)62267-5.

Nielsen, M., Lundegaard, C., Worning, P., Lauemoller, S.L., Lamberth, K., Buus, S., Brunak, S., and Lund, O. (2003). Reliable prediction of T-cell epitopes using neural networks with novel sequence representations. Protein Sci. *12*, 1007–1017. https://doi.org/10.1110/ps.0239403.

O'Driscoll, M., Ribeiro Dos Santos, G., Wang, L., Cummings, D.A.T., Azman, A.S., Paireau, J., Fontanet, A., Cauchemez, S., and Salje, H. (2021). Age-specific mortality and immunity patterns of SARS-CoV-2. Nature *590*, 140–145. https://doi.org/10.1038/s41586-020-2918-0.

Orange, J.S. (2013). Natural killer cell deficiency. J. Allergy Clin. Immunol. *132*, 515–525. https://doi.org/10.1016/j.jaci.2013.07.020.

Osman, M., Faridi, R.M., Sligl, W., Shabani-Rad, M.T., Dharmani-Khan, P., Parker, A., Kalra, A., Tripathi, M.B., Storek, J., Cohen Tervaert, J.W., and Khan, F.M. (2020). Impaired natural killer cell counts and cytolytic activity in patients with severe COVID-19. Blood Adv. *4*, 5035–5039. https://doi.org/10.1182/bloodadvances.2020002650.

Parikh, B.A., Bern, M.D., Piersma, S.J., Yang, L., Beckman, D.L., Poursine-Laurent, J., Plougastel-Douglas, B., and Yokoyama, W.M. (2020). Control of viral infection by natural killer cell inhibitory receptors. Cell Rep. *32*, 107969. https://doi.org/10.1016/j.celrep.2020.107969.

Peters, B., and Sette, A. (2005). Generating quantitative models describing the sequence specificity of biological processes with the stabilized matrix method. BMC Bioinf. *6*, 132. https://doi.org/10.1186/1471-2105-6-132.

Petrie, E.J., Clements, C.S., Lin, J., Sullivan, L.C., Johnson, D., Huyton, T., Heroux, A., Hoare, H.L., Beddoe, T., Reid, H.H., et al. (2008). CD94-NKG2A recognition of human leukocyte antigen (HLA)-E bound to an HLA class I leader sequence. J. Exp. Med. *205*, 725–735. https://doi.org/10.1084/jem.20072525.

Reefman, E., Kay, J.G., Wood, S.M., Offenhauser, C., Brown, D.L., Roy, S., Stanley, A.C., Low, P.C., Manderson, A.P., and Stow, J.L. (2010). Cytokine secretion is distinct from secretion of cytotoxic granules in NK cells. J. Immunol. *184*, 4852–4862. https://doi.org/10.4049/jimmunol.0803954.

Rendeiro, A.F., Casano, J., Vorkas, C.K., Singh, H., Morales, A., DeSimone, R.A., Ellsworth, G.B., Soave, R., Kapadia, S.N., Saito, K., et al. (2020). Longitudinal immune profiling of mild and severe COVID-19 reveals innate and adaptive immune dysfunction and provides an early prediction tool for clinical progression. Preprint at medRxiv. https://doi.org/10.1101/2020.09.08.20189092.

Roe, D.R., and Cheatham, T.E., 3rd. (2013). PTRAJ and CPPTRAJ: software for processing and analysis of molecular dynamics trajectory data. J. Chem. Theor. Comput *9*, 3084–3095. https://doi.org/10.1021/ct400341p.

Sahoo, D., Katkar, G.D., Khandelwal, S., Behroozikhah, M., Claire, A., Castillo, V., Tindle, C., Fuller, M., Taheri, S., Rogers, T.F., et al. (2021). AI-guided discovery of the invariant host response to viral pandemics. EBioMedicine *68*, 103390. https://doi.org/10.1016/j.ebiom.2021.103390.

Schroder, K., Hertzog, P.J., Ravasi, T., and Hume, D.A. (2004). Interferon-gamma: an overview of signals, mechanisms and functions. J. Leukoc. Biol. *75*, 163–189. https://doi.org/10.1189/jlb.0603252.

Schultze, J.L., and Aschenbrenner, A.C. (2021). COVID-19 and the human innate immune system. Cell *184*, 1671–1692. https://doi.org/10.1016/j.cell.2021.02.029.

Sette, A., and Crotty, S. (2021). Adaptive immunity to SARS-CoV-2 and COVID-19. Cell *184*, 861–880. https://doi.org/10.1016/j.cell.2021.01.007.

Severe Covid-19 GWAS Group; Ellinghaus, D., Degenhardt, F., Bujanda, L., Buti, M., Albillos, A., Invernizzi, P., Fernandez, J., Prati, D., Baselli, G., et al. (2020). Genomewide association study of severe covid-19 with respiratory failure. New Engl. J. Med. *383*, 1522–1534. https://doi.org/10.1056/NEJMoa2020283.

Sidney, J., Assarsson, E., Moore, C., Ngo, S., Pinilla, C., Sette, A., and Peters, B. (2008). Quantitative peptide binding motifs for 19 human and mouse MHC class I molecules derived using positional scanning combinatorial peptide libraries. Immunome Res. *4*, 2. https://doi.org/10.1186/1745-7580-4-2.

Sievers, F., Wilm, A., Dineen, D., Gibson, T.J., Karplus, K., Li, W., Lopez, R., McWilliam, H., Remmert, M., Soding, J., et al. (2011). Fast, scalable generation of high-quality protein multiple sequence alignments using Clustal Omega. Mol. Syst. Biol. *7*, 539. https://doi.org/10.1038/msb.2011.75.

Subramanian, A., Tamayo, P., Mootha, V.K., Mukherjee, S., Ebert, B.L., Gillette, M.A., Paulovich, A., Pomeroy, S.L., Golub, T.R., Lander, E.S., and Mesirov, J.P. (2005). Gene set enrichment analysis: a knowledge-based approach for interpreting genome-wide expression profiles. Proc. Natl. Acad. Sci. U S A *102*, 15545–15550. https://doi.org/10.1073/pnas.0506580102.

Tomasec, P., Braud, V.M., Rickards, C., Powell, M.B., McSharry, B.P., Gadola, S., Cerundolo, V., Borysiewicz, L.K., McMichael, A.J., and Wilkinson, G.W. (2000). Surface expression of HLA-E, an inhibitor of natural killer cells, enhanced by human cytomegalovirus gpUL40. Science *287*, 1031. https://doi.org/10.1126/science.287.5455.1031.

Traag, V.A., Waltman, L., and van Eck, N.J. (2019). From Louvain to Leiden: guaranteeing well-connected communities. Sci. Rep. *9*, 5233. https://doi.org/10.1038/s41598-019-41695-z.

Ulbrecht, M., Martinozzi, S., Grzeschik, M., Hengel, H., Ellwart, J.W., Pla, M., and Weiss, E.H. (2000). Cutting edge: the human cytomegalovirus UL40 gene product contains a ligand for HLA-E and prevents NK cell-mediated lysis. J. Immunol. *164*, 5019–5022. https://doi.org/10.4049/jimmunol.164.10.5019.

V'Kovski, P., Kratzel, A., Steiner, S., Stalder, H., and Thiel, V. (2021). Coronavirus biology and replication: implications for SARS-CoV-2. Nat. Rev. Microbiol. *19*, 155–170. https://doi.org/10.1038/s41579-020-00468-6.

Varchetta, S., Mele, D., Oliviero, B., Mantovani, S., Ludovisi, S., Cerino, A., Bruno, R., Castelli, A., Mosconi, M., Vecchia, M., et al. (2021). Unique immunological profile in patients with COVID-19. Cell Mol. Immunol. *18*, 604–612. https://doi.org/10.1038/s41423-020-00557-9.

Vidal, S.M., and Lanier, L.L. (2006). NK cell recognition of mouse cytomegalovirus-infected cells. Curr. Top. Microbiol. Immunol. *298*, 183–206. https://doi.org/10.1007/3-540-27743-9_10.

Viechtbauer, W. (2010). Conducting meta-analyses in R with the metafor package. J. Stat. Softw. *36*, 48. https://doi.org/10.18637/jss.v036.i03.

Wilk, A.J., Lee, M.J., Wei, B., Parks, B., Pi, R., Martinez-Colon, G.J., Ranganath, T., Zhao, N.Q., Taylor, S., Becker, W., et al. (2021). Multi-omic profiling reveals widespread dysregulation of innate immunity and hematopoiesis in COVID-19. J. Exp. Med. *218*, e20210582. https://doi.org/10.1084/jem.20210582.

Wilk, A.J., Rustagi, A., Zhao, N.Q., Roque, J., Martinez-Colon, G.J., McKechnie, J.L., Ivison, G.T., Ranganath, T., Vergara, R., Hollis, T., et al. (2020). A single-cell atlas of the peripheral immune response in patients with severe COVID-19. Nat. Med. *26*, 1070–1076. https://doi.org/10.1038/s41591-020-0944-y.

Witkowski, M., Tizian, C., Ferreira-Gomes, M., Niemeyer, D., Jones, T.C., Heinrich, F., Frischbutter, S., Angermair, S., Hohnstein, T., Mattiola, I., et al. (2021). Untimely TGFbeta responses in COVID-19 limit antiviral functions of NK cells. Nature *600*, 295–301. https://doi.org/10.1038/s41586-021-04142-6.

Wolf, F.A., Angerer, P., and Theis, F.J. (2018). SCANPY: large-scale single-cell gene expression data analysis. Genome Biol. *19*, 15. https://doi.org/10.1186/s13059-017-1382-0.

Yang, C., Siebert, J.R., Burns, R., Gerbec, Z.J., Bonacci, B., Rymaszewski, A., Rau, M., Riese, M.J., Rao, S., Carlson, K.S., et al. (2019). Heterogeneity of

human bone marrow and blood natural killer cells defined by single-cell transcriptome. Nat. Commun. *10*, 3931. https://doi.org/10.1038/s41467-019-11947-7.

Zenarruzabeitia, O., Astarloa-Pando, G., Terren, I., Orrantia, A., Perez-Garay, R., Seijas-Betolaza, I., Nieto-Arana, J., Imaz-Ayo, N., Perez-Fernandez, S., Arana-Arri, E., and Borrego, F. (2021). T cell activation, highly armed cytotoxic cells and a shift in monocytes CD300 receptors expression is characteristic of patients with severe COVID-19. Front. Immunol. *12*, 655934. https://doi.org/10.3389/fimmu.2021.655934.

Zhang, Y., Chen, Y., Li, Y., Huang, F., Luo, B., Yuan, Y., Xia, B., Ma, X., Yang, T., Yu, F., et al. (2021). The ORF8 protein of SARS-CoV-2 mediates immune evasion through down-regulating MHC-Iota. Proc. Natl. Acad. Sci. U S A *118*, e2024202118. https://doi.org/10.1073/pnas.2024202118.

Zheng, M., Gao, Y., Wang, G., Song, G., Liu, S., Sun, D., Xu, Y., and Tian, Z. (2020). Functional exhaustion of antiviral lymphocytes in COVID-19 patients. Cell Mol. Immunol. *17*, 533–535. https://doi.org/10.1038/s41423-020-0402-2.

## STAR★METHODS

### KEY RESOURCES TABLE

| REAGENT or RESOURCE | SOURCE | IDENTIFIER |
|---|---|---|
| **Antibodies** | | |
| anti-HLA class I-FITC (W6/32) | BioLegend | AB_314873 |
| anti-HLA-E-PE (3D12) | BioLegend | AB_1659249 |
| anti-HLA-E (3D12) | ThermoFisher | AB_1210774 |
| anti-CD14-V500 (M5E2) | BD Biosciences | AB_10611856 |
| anti-CD19-BV570 (HIB19) | BioLegend | AB_2563606 |
| anti-CD3-PE-Cy5 (UCHT1) | Beckman Coulter | AB_2827419 |
| anti-CD56-BUV737 (NCAM16.2) | BD Biosciences | AB_2860005 |
| anti-CD56-ECD (N901) | Beckman Coulter | AB_2750853 |
| anti-CD16-BV786 (3G8) | BioLegend | AB_2563803 |
| anti-CD57-PacificBlue (HCD57) | BioLegend | AB_2063198 |
| anti-NKG2A-ViobrightFITC (REA110) | Miltenyi Biotec | AB_2726173 |
| anti-NKG2C-PE (REA205) | Miltenyi Biotec | AB_2751835 |
| anti-KIR2DL1-APC (REA284) | Miltenyi Biotec | AB_2752101 |
| anti-KIR2DL3-Biotin (REA147) | Miltenyi Biotec | AB_2655344 |
| anti-KIR3DL1-APC-Fire750 (DX9) | BioLegend | AB_2687394 |
| anti-KIR2DL1/DS1-PE-Cy7 (EB6) | Beckman Coulter | AB_2801261 |
| anti-KIR2DL2/L3/S2-PE-Cy5.5 (GL183) | Beckman Coulter | AB_2857331 |
| anti-CD107a-BUV395 (H3A4) | BD Biosciences | AB_2739073 |
| anti-TNF-BV650 (MAb11) | BioLegend | AB_2562741 |
| anti-IFN-γ-Alexa700 (B27) | BD Biosciences | AB_396977 |
| anti-CD94 (#131412) | R&D Systems | AB_2234380 |
| **Bacterial and virus strains** | | |
| SARS-CoV-2/human/SWE/01/2020 | Public Health Agency of Sweden | MT093571.1 |
| **Biological samples** | | |
| Buffy coats from healthy donors | Department of Clinical Immunology and Transfusion Medicine, Karolinska Institute | N/A |
| Cohort of patients with COVID-19 and healthy controls | Maucourant et al. 2020; Table S1 | https://covid19cellatlas.com/ |
| **Chemicals, peptides, and recombinant proteins** | | |
| $pp65_{495\text{-}503}$ (NLVPMVATV) | Peptides&Elephants | EP04509_1 |
| HLA-$C_{3\text{-}11}$ (VMAPRTLIL) | Peptides&Elephants | EP06244_1 |
| $Nsp13_{232\text{-}240}$ (VMPLSAPTL) | Peptides&Elephants | N/A |
| $S_{269\text{-}277}$ (YLQPRTFLL) | Peptides&Elephants | N/A |
| $Nsp6_{114\text{-}122}$ (VMYASAVVL) | Peptides&Elephants | N/A |
| Biotinylated Human NKG2A&CD94 Protein | Acro Biosystems | NC4-H82F5 |
| Gibco Human IL-15 Recombinant Protein | ThermoFisher | PHC9151 |
| Recombinant Human IFN-Alpha2a | PBL Assay Science | 11101-2 |
| **Critical commercial assays** | | |
| BD Cytofix/Cytoperm™ | BD Biosciences | AB_2869008 |
| RNeasy Micro Plus Kit | Qiagen | 74034 |
| SARS-CoV-2 (2019-nCoV) CDC qPCR Probe Assay, RUO Kit | IDT | 10006713 |
| TaqPath™ 1-Step RT-qPCR Master Mix, CG | ThermoFisher | A15299 |

(*Continued on next page*)

*Continued*

| REAGENT or RESOURCE | SOURCE | IDENTIFIER |
|---|---|---|
| **Deposited data** | | |
| HCMV pp65 protein sequence | UniProt | P06725 |
| HLA-C*01:02:01:01 protein sequence | IMGT | HLA00401 |
| SARS-CoV-2 isolate Wuhan-Hu-1 genomic sequence | GenBank | NC_045512.2 |
| Human CD94/NKG2A in complex with HLA-E crystal structure | PDB | 3CDG |
| SARS coronavirus Tor2 genomic sequence | GenBank | NC_004718.3 |
| Human coronavirus HKU1 genomic sequence | GenBank | NC_006577.2 |
| Human coronavirus OC43 genomic sequence | GenBank | AY391777.1 |
| Human coronavirus NL63 genomic sequence | GenBank | NC_005831.2 |
| Human coronavirus 229E genomic sequence | GenBank | NC_002645.1 |
| Bat SARS-like coronavirus isolate Rf4092 genomic sequence | GenBank | KY417145.1 |
| Bat coronavirus Cp/Yunnan2011 genomic sequence | GenBank | JX993988.1 |
| Bat SARS-like coronavirus isolate Rs4084 genomic sequence | GenBank | KY417144.1 |
| Bat SARS coronavirus HKU3-7 genomic sequence | GenBank | GQ153542.1 |
| Bat coronavirus (BtCoV/279/2005) genomic sequence | GenBank | DQ648857.1 |
| Bat SARS-like coronavirus RsSHC014 genomic sequence | GenBank | KC881005.1 |
| Pangolin coronavirus isolate MP789 genomic sequence | GenBank | MT084071.1 |
| Pangolin coronavirus isolate PCoV_GX-P1E genomic sequence | GenBank | MT040334.1 |
| Pangolin coronavirus isolate PCoV_GX-P4L genomic sequence | GenBank | MT040333.1 |
| Bat SARS-like coronavirus isolate bat-SL-CoVZXC21 genomic sequence | GenBank | MG772934.1 |
| Bat SARS-like coronavirus isolate bat-SL-CoVZC45 genomic sequence | GenBank | MG772933.1 |
| Bat coronavirus RaTG13 genomic sequence | GenBank | MN996532.2 |
| SARS-CoV-2/human/SWE/01/2020 genomic sequence | GenBank | MT093571.1 |
| scRNA-seq dataset of immune cells from BALF of a healthy control | Morse et al., 2019 | GSE128033 |
| scRNA-seq dataset of immune cells from BALF of patients with COVID-19 and healthy controls | Liao et al., 2020 | GSE145926 |
| **Experimental models: Cell lines** | | |
| K562/HLA-E | Ulbrecht et al., 2000 | N/A |
| A549-hACE2 | O. Fernandez-Capetillo, Karolinska Insitute | N/A |
| **Software and algorithms** | | |
| NetMHC 4.0 | Andreatta and Nielsen, 2016; Nielsen et al., 2003 | https://services.healthtech.dtu.dk/service.php?NetMHC-4.0 |
| IEDB | Peters and Sette, 2005; Sidney et al., 2008 | http://tools.iedb.org/processing/ |
| FlowJo X | BD Biosciences | SCR_008520; https://www.flowjo.com/ |

(*Continued on next page*)

*Continued*

| REAGENT or RESOURCE | SOURCE | IDENTIFIER |
|---|---|---|
| Prime | Jacobson et al., 2004 | SCR_014887; https://www.schrodinger.com/products/prime |
| Amber18 | Case et al., 2005 | SCR_014230; https://ambermd.org/ |
| Clustal Omega | EMBL-EBI | SCR_001591; https://www.ebi.ac.uk/Tools/msa/clustalo/ |
| iTOL | EMBL | SCR_018174; https://itol.embl.de/ |
| SCANPY | Wolf et al., 2018 | SCR_018139; https://scanpy.readthedocs.io/ |
| GSEAPY | Subramanian et al., 2005 | https://gseapy.readthedocs.io/ |
| R | The R Foundation | SCR_001905; https://www.rproject.org/ |
| GraphPad Prism | GraphPad Software, LLC. | SCR_002798; https://www.graphpad.com/ |

## RESOURCE AVAILABILITY

### Lead contact

Further information and requests for resources and reagents should be directed to and will be fulfilled by the lead contact, Quirin Hammer (quirin.hammer@ki.se).

### Materials availability

This study did not generate new unique reagents.

### Data and code availability

- The data reported in this study will be shared by the lead contact upon reasonable request. All existing data used in this study including protein sequences for HLA-E binding predictions, crystal structures for MD simulations, genomic sequences for sequence identity comparisons, and scRNA-seq datasets are publicly available. Databanks and corresponding identifiers are listed in the key resources table.
- This study did not generate new code.
- Any additional information required to reanalyze the data reported in this paper is available from the lead contact upon request.

## EXPERIMENTAL MODEL AND SUBJECT DETAILS

### Human subjects

Buffy coats from healthy donors were obtained from the Department of Clinical Immunology and Transfusion Medicine, Karolinska Institutet as approved by the Ethical Review Board Stockholm (DNR 2020-05289). Due to data protection regulations, neither age nor gender of healthy donors are available. PBMC were isolated from buffy coats with standard density gradient centrifugation, cryopreserved in FBS containing 10% (v/v) DMSO, and stored in the vapor phase of liquid nitrogen.

The cohort of patients with COVID-19 of the Karolinska COVID-19 Immune Atlas has been previously described (Maucourant et al., 2020) and characteristics of the patients are available in Table S1. Further details can be found at https://covid19cellatlas.com/.

### Culture conditions for *in vitro* systems

All primary cells and cell lines were maintained at 37°C and 5% $CO_2$ in a humidified incubator. The relevant media including supplements are described in the corresponding method details.

### Cell lines

K562 cells expressing HLA-E*01:03 (K562/HLA-E cells; generated by E. Weiss, Ludwig Maximilian University (Ulbrecht et al., 2000)) were maintained in complete RPMI (RPMI-1640 supplemented with 2 mM glutamine, 10% [v/v] FBS, 100 U/ml penicillin, and 100 μg/ml streptomycin; all Gibco) in the presence of 1 mg/ml G418 (Gibco).

A549 cells expressing ACE2 (A549-hACE2; generated by O. Fernandez-Capetillo, Karolinska Institute) were maintained in complete MEM (MEM supplemented with 2 mM glutamine, 7.5% [v/v] FBS, 100 U/ml penicillin, and 100 μg/ml streptomycin; all Gibco).

Cell lines were routinely tested for presence of Mycoplasma (Mycoplasmacheck, Eurofins Genomics). Cell line authentication was not performed in this study.

## METHOD DETAILS

### HLA-E binding prediction

Binding of nonamers from HCMV pp65 (UniProt P06725), HLA-C*01:02:01 (IMGT HLA00401), and ORFeome of SARS-CoV-2 (isolate Wuhan-Hu1; GenBank NC_045512.2) to HLA-E*01:01 was predicted *in silico* using NetMHC 4.0 (Andreatta and Nielsen, 2016; Nielsen et al., 2003). Binding scores were obtained by dividing 100 by the predicted binding affinity in nM. Alternatively, binding and processing predictions were made using the Immune Epitope Database (IEDB) analysis resource (Peters and Sette, 2005; Sidney et al., 2008) on 01/28/2021 for HLA-E*01:01 with standard settings (immune proteasome; maximum precursor extension of 1; alpha factor of 0.2).

### HLA-E surface stabilization

HLA-E surface stabilization was performed as described previously (Hammer et al., 2018a). In brief, synthetic peptides of $\geq$95% purity (Peptides&Elephants) were reconstituted in sterile water and K562/HLA-E cells cultured at $2x10^6$ cells per ml in serum-free Opti-MEM (ThermoFisher) were treated with 300 μM synthetic peptides at 37°C over-night (12-18 h). Peptide-pulsed cells were either washed with complete RPMI and used in assays with NK cells or stained for flow cytometric analysis of HLA-E. For assessment of HLA-E/peptide stability with pulse-chase experiments, K562/HLA-E were pulsed as above, washed twice, and resuspended in Opti-MEM without peptide. HLA-E surface levels were monitored by flow cytometry at indicated time points. For assessment of receptor binding, peptide-pulsed K562/HLA-E were first incubated with 50 μg/ml recombinant biotinylated CD94/NKG2A (Acro Biosystems) for 20 min on ice, followed by detection with Streptavidin-BV711 (BD Biosciences) and staining of HLA-E.

### Flow cytometry

Flow cytometric stainings and analyses were performed following established guidelines (Cossarizza et al., 2017). In brief, cell suspensions were incubated with combinations of fluorochrome-conjugated antibodies (key resources table) at optimized concentrations in PBS for 20 min at RT. Viable cells were identified with LIVE/DEAD Fixable Aqua Dead Cell Stain Kit or Fixable Viability Dye eFluor 780 (both ThermoFisher). Streptavidin-BV711 (BD Biosciences) was used as secondary reagent in combination with biotinylated primary reagents. All samples were fixed before acquisition using BD Cytofix/Cytoperm (BD Biosciences) according to the manufacturer's instructions and, if indicated, intracellular proteins were stained with fluorochrome-conjugated antibodies in Perm/Wash buffer (BD Biosciences) for 30 min at 4°C. Samples were acquired on an LSR Fortessa flow cytometer (BD Biosciences) and analyzed with FlowJo v10.7.1 (BD Biosciences).

### Molecular dynamics simulations

The crystallographic structure of HLA-E (Petrie et al., 2008) was retrieved from Protein Data Bank (PDB) (Berman et al., 2000) accession 3CDG and used as template to build HLA-E*01:03/peptide complexes by homology modelling with Prime (Jacobson et al., 2004). MD simulations were carried out with Amber18 (Case et al., 2005) using the ff14SB force field (Maier et al., 2015). All systems were solvated in a rectangular box of explicit TIP3P type water molecules, neutralized with the addition of counter-ions, and relaxed through energy minimization. First, solvent was relaxed by keeping the protein fixed for 5,000 steps of which 1,500 steps used the Steepest Descend Algorithm (SDA) and 3,500 steps used the Conjugate Gradient Algorithm (CGA). Next, the entire systems were energy minimized for 10,000 steps of which 1,500 steps used SDA and 8,500 steps used CGA. All systems were heated at constant volume from 0 K to 300 K over 1 ns with the Langevin thermostat and density equilibration was performed at constant pressure with the Berendsen barostat for 1 ns. Finally, after a preliminary equilibration of 50 ns, the final MD trajectories were produced in three independent replicas of 500 ns each. MD trajectories were analyzed with CPPTRAJ (Roe and Cheatham, 2013), while the MM-GBSA approach was used to evaluate the delta energy of binding ($\Delta E_b$) of peptides to HLA-E, as well as to decompose it into the main contributions (Miller et al., 2012). MM-GBSA calculations were carried out using the single trajectory approach over 100 frames for each complex and for each MD simulation replica. The peptides' $\Delta E_b$ was computed as the average of three replicas.

### Phylogenetic analyses

To examine phylogenic relationships, the genomic sequences of SARS-CoV-2 (isolate Wuhan-Hu1; NC_045512.2), SARS-CoV-1 (Tor2; NC_004718.3), HCoV-HKU1 (NC_006577.2), HCoV-OC43 (AY391777.1), HCoV-NL63 (NC_005831.2), and HCoV-229E (NC_002645.1) as well as of sarbecovirus isolates from bats and pangolins (see Figure S2A and key resources table for accession numbers) were obtained from GenBank and compared by multiple sequence alignments with Clustalω (Sievers et al., 2011) at EMBL-EBI (Madeira et al., 2019). Phylograms based on alignments were generated with iTOL (Letunic and Bork, 2021).

### Cellular thermal shift assay

Cellular thermal shift assays (CETSA) were performed according to standard protocols (Martinez Molina et al., 2013). Briefly, cellular extract from K562/HLA-E cells was freshly prepared in RIPA buffer (10 mM Tris HCl pH 7.4, 150 mM NaCl, 1% Igepal, 1% sodium deoxycholate, 0.1% sodium dodecyl sulfate, 0,1% glycerol, protease and phosphatase inhibitors cocktail, and 2 mM 1,4-dithiothreitol). Cell homogenization was performed by 3 freeze-thawing cycles and the soluble fraction was separated from debris by centrifugation at 20,000 x g for 20 min at 4°C. For each CETSA experiment, a single cell lysate obtained from $1x10^7$ cells was divided

into two aliquots, with one aliquot being treated with 0.5 mM peptide and the other one exposed to water as solvent. After 30 min incubation at RT, the lysates were heated individually to 56°C for 3 min followed by 3 min cooling at RT. The heated lysates were centrifuged at 20,000 x *g* for 20 min at 4°C and supernatants were analyzed by western blotting with an anti-HLA-E antibody (clone 3D12, ThermoFisher).

### HLA-E tetramers

HLA-E:01*03 tetramers refolded with HLA-$C_{3\text{-}11}$ or $Nsp13_{232\text{-}240}$ and conjugated to PE were obtained from the NIH Tetramer Core Facility. Thawed PBMC were incubated with tetramers diluted 1:100 in PBS for 15 min at RT in the absence or presence of 20 μg/ml blocking anti-CD94 antibodies (clone #131412, R&D Systems). Without washing, a mix of fluorochrome-conjugated antibodies was added and incubated for additional 15 min at RT. NK cells were identified as single viable $CD14^-$ $CD19^-$ $CD3^-$ $CD56^{dim}$ cells and further gated for sub-populations as indicated.

### Functional assays

For functional assays, cryopreserved PBMC were thawed in the presence of 25 U/ml Benzonase (Merck Millipore) and NK cells were purified by magnetic isolation (NK Cell Isolation Kit, Miltenyi Biotec) according to the manufacturer's instructions. Purified NK cells were rested in complete RPMI over-night (12-18 h) and $5x10^4$ NK cells were co-cultured with $5x10^4$ peptide-pulsed K562/HLA-E in 200 μl complete RPMI in V-bottom 96-well plates for 6 h at 37°C. Peptides were present during the co-culture at 300 μM. To detect degranulation, anti-CD107a antibodies were added at the start of the co-culture and GolgiStop (containing monensin) as well as GolgiPlug (containing Brefeldin A, both BD Biosciences) were added after 1 h. After 6 h total co-culture, the cells were stained for surface markers and fixed and permeabilized (BD Cytofix/Cytoperm, BD Biosciences) for intracellular detection of IFN-γ and TNF. NK cells were identified as single viable $CD14^-$ $CD19^-$ $CD3^-$ $CD56^{dim/bright}$ cells and further gated for sub-populations as indicated.

### Re-analysis of NK cell activation in a previously described patient cohort

The cohort of patients with COVID-19 that was used for the analysis of NK cell activation has been previously described (Maucourant et al., 2020). In brief, 27 patients with SARS-CoV-2 PCR-confirmed moderate or severe COVID-19 admitted to the Karolinska University Hospital, Stockholm, Sweden and 17 healthy controls were included in the study as part of the Karolinska COVID-19 Immune Atlas (Table S1 and https://covid19cellatlas.com/). Ethical approval was obtained from the Ethical Review Board Stockholm (DNR 2020-01558). Two patients with COVID-19 were excluded due to low NK cell counts. Flow cytometric analysis was performed by identifying NK cells as single viable $CD14^-$ $CD19^-$ $CD123^-$ $CD45^+$ $CD3^-$ $CD56^{dim/bright}$ cells and further gated for sub-populations as indicated.

### Re-analysis of NK cell activity in a previously reported single-cell RNA sequencing dataset

Publicly available single-cell RNA sequencing (scRNA-seq) data of immune cells from BALF of four healthy controls and 13 patients with COVID-19 were acquired from GSE128033 and GSE145926 (Liao et al., 2020; Morse et al., 2019). Data were analyzed with SCANPY (Wolf et al., 2018) using the annotation provided by Liao et al. (Liao et al., 2020). Gene set enrichment analysis (GSEA) of an inflammatory NK cell signature (Yang et al., 2019) along *KLRC1* expression levels was performed with GSEAPY (Subramanian et al., 2005) and genes that positively correlated with *KLRC1* expression in COVID-19 samples were further integrated into an inflammatory score (Table S2). Uniform Manifold Approximation and Projection (UMAP) embedding was computed in SCANPY and clustering was performed using the Leiden algorithm (Traag et al., 2019).

### Genetic association analysis of *HLA-B –21*

Genetic association of the *HLA-B –21* polymorphism with severe respiratory COVID-19 was tested in a subgroup of the cohort of the Severe Covid-19 GWAS group (Degenhardt et al., 2021). Specifically, a case-only design was chosen, in which 3,193 individuals with severe COVID-19 with respiratory failure from Germany/Austria, Italy and Spain were analyzed. Severe COVID-19 with respiratory failure was defined as in the original study as hospitalization due to an RNA polymerase chain reaction (PCR)-confirmed infection with SARS-CoV-2, with need of respiratory support by either oxygen supplementation or mechanical ventilation. Details on study design and patient groups are described in Degenhardt et al. (Degenhardt et al., 2021) and Ellinghaus et al. (Severe Covid-19 GWAS Group et al., 2020). In brief, all COVID-19 cases were categorized into oxygen supplementation or mechanical ventilation as an indicator for disease severity, resulting in a total of 1,282 individuals with oxygen supplementation and 1,911 individuals with mechanical ventilation. Imputed HLA allele information was available for the 3,193 individuals at 2- and 4-digit G group level, from which we extracted *HLA-B* alleles. Presence of methionine (*M*) or threonine (*T*) at *HLA-B –21* was inferred for all individuals from 2- digit *HLA-B* allele genotypes as follows: individuals carrying two copies of any of the B*07, B*08, B*13-B*15, B*18, B*27, B*35, B*37-B*42, B*44-B*59, B*67, B*73, B*78, B*81-B*83 (Horowitz et al., 2016) were assigned *M*/*M*, individuals carrying any other B alleles were assigned *T*/*T*, individuals carrying alleles from both groups were assigned *M*/*T*. The association of *HLA-B –21* with COVID-19 severity, i.e., oxygen supplementation vs. mechanical ventilation, in the German/Austrian, Spanish, and Italian cohorts was then tested using logistic regression, including age, $age^2$, sex, age*sex. and the first 10 principal components (PCs) derived from principal component analysis (PCA) of whole-genome SNP information and using a recessive model of inheritance (*M*/*M* vs.

*T/M* + *T/T*) in R. This was followed by a fixed-effects inverse variance-weighted meta-analysis of estimates and their standard error across the three populations using the metafor (Viechtbauer, 2010) package in R.

### Virus inhibition assay

To determine the anti-viral capacity of NK cell subsets, $5x10^4$ A549-hACE2 cells were plated in 48 well plates and infected with SARS-CoV-2 (isolate SARS-CoV-2/human/SWE/01/2020; GenBank accession: MT093571.1) at MOI=0.1 in complete MEM for 1 h. Cells were washed and maintained in complete MEM following infection. Magnetically isolated NK cells were stained for viability, CD3, CD56, and NKG2A and sorted for single viable $CD3^-$ $CD56^{dim}$ $NKG2A^-$ and $NKG2A^+$ cells using an MA900 cell sorter (Sony). Sorted NK cells were rested in complete RPMI supplemented with 5 ng/ml IL-15 (Gibco) and 5,000 U/ml IFN-$\alpha$2a (PBL Assay Science) overnight (15-18 h). The next day, NK cells were washed two times with medium to remove cytokines and subsequently co-cultured with SARS-CoV-2-infected A549-hACE2 in complete MEM at indicated E:T ratios starting at 1 h post-infection. At 24 h post-infection, the cultures were washed twice with PBS to remove NK cells and total RNA was isolated from adherent A549-hACE2 cells using the RNeasy Micro Plus Kit (Qiagen) according to the manufacturer's instructions. Viral load was determined with the CDC nCoV-2019 N1 assay (IDT) using TaqPath™ 1-Step RT-qPCR Master Mix, QuantStudio 5, and ThermoFisher Connect analysis platform (all ThermoFisher).

For assessment of HLA-E and HLA class I expression, A549-hACE2 cells were dissociated at 24 h post infection using trypsin-EDTA solution (Sigma-Aldrich), stained for flow cytometric analyses as above, and stored in PBS containing 0.5% (v/v) paraformaldehyde (Electron Microscopy Sciences) until acquisition.

## QUANTIFICATION AND STATISTICAL ANALYSIS

Statistical parameters such as sample size, number of performed experiments, employed statistical tests, and statistical significance are reported in the figures and figure legends. In general, two groups of paired or unpaired samples were analyzed with the two-tailed Wilcoxon test or the Mann-Whitney *U* test, respectively. Three or more groups of paired samples were analyzed with the Friedman test with Dunn's post-test to correct for multiple comparisons. Paired samples with two variables (e.g., different peptides and different concentrations) were analyzed with repeated-measured two-way ANOVA with Bonferroni correction. If not stated otherwise, statistical analyses were performed in Prism 9 (GraphPad Software) with a confidence level of 0.95 and $p > 0.05$ was considered not significant (ns).